MASTERARBEIT | MASTER'S THESIS

Titel | Title

The analysis of the different allosteric pathways in mGIRK2wv and mGIRK2wt

verfasst von | submitted by

Janka Müller BSc

angestrebter akademischer Grad | in partial fulfilment of the requirements for the degree of

Magistra pharmaciae (Mag. pharm.)

Wien | Vienna, 2025

Studienkennzahl lt. Studienblatt | Degree programme code as it appears on the student record sheet:	UA 066 605
Studienrichtung lt. Studienblatt | Degree programme as it appears on the student record sheet:	Masterstudium Pharmazie
Betreut von | Supervisor:	Assoz. Prof. Mag. Dr. Anna Weinzinger Privatdoz.

Table of Contents

Acknowledgment

I would like to express my profound gratitude to Assoc. Prof. Priv. Doz. Dr. Anna Weinzinger for granting me the opportunity to participate in her research group and for providing me with supervision throughout the research process. Secondly, I would like to express my gratitude to Theres Friascher for her consistent support, mentorship throughout the research process. Her readiness to assist whenever I faced challenges was invaluable.

In addition, I would like to express my sincere gratitude to my family and close friends for their unwavering support throughout my academic endeavours. Finally, I would like to acknowledge the invaluable contributions of all those who have assisted me in my academic journey.

Abstract

G protein-gated inwardly rectifying potassium (GIRK) channels are key regulators of electrical excitability in the heart and brain, where they generate slow inhibitory postsynaptic potentials. Aberrant GIRK channel function has been implicated in various pathophysiological conditions, often arising from mutations that alter gating mechanisms or ion selectivity. Keppen-Lubinsky syndrome (KPLBS) is a rare neurodevelopmental disorder caused by dominant mutations in the *KCNJ6* gene, which encodes the GIRK2 subunit. A corresponding mutation in the selectivity filter (G156S) has been studied in the weaver mouse model that results in a constitutively active, non-selective channel that is unresponsive to G protein signaling and allows the permeation of non-potassium ions. Molecular dynamics simulations combined with electrophysiological experiments have revealed an allosteric connection between the selectivity filter and the Gβγ-binding site, suggesting that disruption of this coupling underlies the mutant phenotype. To further investigate the allosteric pathways distinguishing wild-type (mGIRK2wt) and mutant (mGIRK2wv) GIRK2 channels, this study applies the get Residue Interaction Energies and Networks (gRINN) framework to identify residues critical for channel dynamics, function, and regulation. The analysis of betweenness and closeness centrality showed no clear difference between mGIRK2wv and mGIRK2wt, however shortest pathway analysis revealed a cooperation in communication pathways between adjacent mGIRK2wt subunits that is abolished in mGIRK2wv. We propose that this weakened subunit cooperation may underlie the aberrant channel activity observed in the G156S weaver mouse model. However further experiments are required to confirm this hypothesis.

Zusammnenfassung

G-Protein-gesteuerte einwärts gleichrichtende Kaliumkanäle (GIRK) sind wichtige Regulatoren der elektrischen Erregbarkeit im Herzen und im Gehirn, wo sie langsame hemmende postsynaptische Potenziale erzeugen. Eine gestörte Funktion des GIRK-Kanals wird mit verschiedenen pathophysiologischen Zuständen in Verbindung gebracht, die häufig auf Mutationen zurückzuführen sind, welche die Gating-Mechanismen verändern oder die Ionenselektivität unterbrechen. Das Keppen-Lubinsky-Syndrom (KPLBS) ist eine seltene neurologische Entwicklungsstörung, die durch dominante Mutationen im KCNJ6-Gen verursacht wird, das für die GIRK2-Untereinheit kodiert. Eine Mutation im Selektivitätsfilter (G156S) wurde im Weaver-Mausmodell untersucht, die zu einem konstitutiv aktiven, nichtselektiven Kanal führt, der nicht auf G-Protein-Signalisierung reagiert und die Permeation von Nicht-Kalium-Ionen ermöglicht. Molekulardynamiksimulationen in Kombination mit elektrophysiologischen Experimenten haben eine allosterische Verbindung zwischen dem Selektivitätsfilter und der Gβγ-Bindungsstelle aufgedeckt, was darauf hindeutet, dass eine Störung dieser Kopplung dem mutanten Phänotyp zugrunde liegt. Um die allosterischen Pfade, die Wildtyp- (mGIRK2wt) und mutierte (mGIRK2wv) GIRK2-Kanäle unterscheiden, weiter zu untersuchen, wendet diese Studie das get Residue Interaction Energies and Networks (gRINN) Framework an, um Residues zu identifizieren, die für die Kanaldynamik, -funktion und -regulierung entscheidend sind. Die Analyse der Betweenness- und Closeness-Zentralität zeigte keinen eindeutigen Unterschied zwischen mGIRK2wv und mGIRK2wt, jedoch ergab die Analyse der kürzesten Pfade eine Kooperation in den Kommunikationspfaden zwischen benachbarten mGIRK2wt-Untereinheiten, die in mGIRK2wv aufgehoben ist. Wir vermuten, dass diese geschwächte Zusammenarbeit der Untereinheiten die Ursache für die gestörte Kanalaktivität im G156S-Weaver-Mausmodell sein könnte. Es sind jedoch weitere Experimente erforderlich, um diese Hypothese zu bestätigen.

List of abbreviations

K+	potassium
Kir	inwardly-rectifying K+ channels
TMD	transmembrane domain
SF	selectivity filter
P-loop	pore loop
CTD	cytoplasmic domain
HBC	helix-bundle crossing
Kv	voltage-gated K+ channel
VSD	voltage sensor domain
Em	membrane potential
Ek	equilibrium potential of K+
GIRK	G protein-gated Kir channels
GCPR	G protein-coupled receptors
PIP2	phosphatidylinositol 4,5-biphosphate
LoF	low of function
GoF	gain of function
GIRK2wv	GIRK2 weaver mouse model
GIRK2wt	GIRK2 wild type model
KPLBS	Keppen-Lubinsky syndrome
OCD	obsessive-compulsive disorder
MD	molecular dynamic
FMA	functional mode analysis
gRINN	get Residue Interaction Energies and Networks
PEN	Protein Energy Network
PSN	Protein Structure Network
GUI	graphical user interfaces
BC	betweenness centrality
CC	closeness centrality

FRET	single molecule fluorescence resonance energy transfer
SSNMR	solid-state nuclear magnetic resonance

1 Literature overview

1.1 Kir channels

In 1949, the research on inward-rectifier potassium (K+) channels began, when Katz described an “anomalous” K+ current in skeletal muscle membrane that rectifies unconventionally, meaning it showed a greater flow into the cell (inward), compared with the already familiar outwardly rectifying K+ current. After his discovery, the anomalously rectifying current, later known as the inwardly rectifying K+ current, became the subject of much investigation into its nature, purpose, and mechanism **(*Lu, 2004; Kurata, 2004*)**.

The family of inwardly-rectifying potassium channels, i.e., Kir channels, are a group of transmembrane proteins that have been found to be expressed in multiple organs and in a wide variety of cells, such as: cardiac myocytes, neurons, blood cells, osteoclast, endothelial cells, glial cells, epithelial cells and oocytes **(*Hibino et al., 2010)***. As a consequence of this extensive physiological appearance, they play important roles in various physiological functions such as controlling the resting membrane potential and the electrical activity in the heart and nerve cells, coupling insulin release from pancreatic beta cells to blood glucose levels, and maintaining K+ homeostasis **(*Lu, 2004; Kurata, 2004*)**.

1.1.1 Kir family

Kir channels are encoded by KCNJ genes. There are currently 16 known KCNJ genes that have been categorized into seven subfamilies (Kir1.x - Kir7.x) and classified into four functional groups ***(Figure 1*) *(Hager,2022; Hibino et al., 2010)***.

I. Classical Kir channels (Kir2.x)
II. G protein-gated Kir channels (Kir3.x)
III. ATP-sensitive K+ channels (Kir6.x)
IV. K+-transport channels (Kir1.x, Kir4.x, Kir5.x, and Kir7.x)

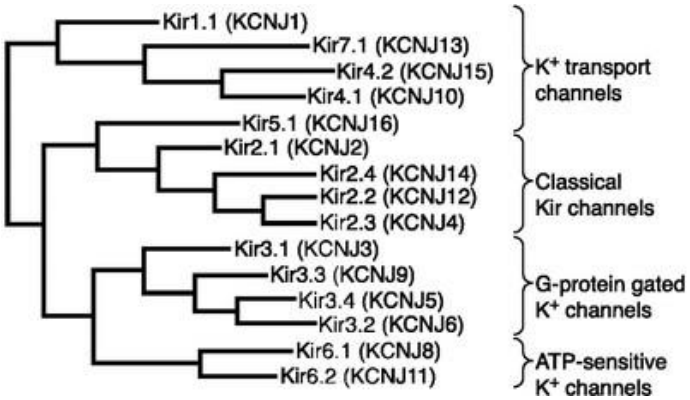

Figure 1: Phylogenetic Analysis of Human Kir Channels. The 15 known subunits of human Kir channels are classified into four distinct functional groups based on their sequence similarities and phylogenetic relationships ***(Source: Hibino, H., Inanobe, A., Furutani, K., Murakami, S., Findlay, I., & Kurachi, Y. (2010). Inwardly rectifying potassium channels: their structure, function, and physiological roles. Physiological reviews, 90(1), 291–366. https://doi.org/10.1152/physrev.00021.2009).***

Sequence homology between subfamilies is 40% but within some subfamilies it increases to about 70%. Functional channels are tetramers of both homomeric and heteromeric combination. Heterotetramers are mostly formed between subunits of the same Kir channel family, for instance Kir3.1 can associate with either Kir3.2, Kir3.3 or Kir3.4 **(*Hibino et al., 2010)***. The Kir subunit combination influences the kinetic properties of the channel. For example, Kir3.1/Kir3.2 heterotetramers display enhanced activity compared to the Kir3.2 homotetramer. In other words, if Kir3.1/Kir3.2 subunits are expressed together, the resulting inward rectifier currents rise significantly ***(Walsh, 2020)***.

1.1.2 Kir Structure

The architecture of eukaryotic Kir channels has been first elucidated by the crystal structures of KirBac, which is the prokaryotic homolog of mammalian Kir channels ***(Zubcevic, 2014)***. Much like KirBac, mammalian Kir channels are tetrameric structures that comprise a transmembrane domain (TMD), consisting of two transmembrane helices called TM1, the outer alpha-helix and TM2, the inner alpha-helix. These membrane-spanning helices are connected by an extracellular turret region, a short pore helix (P) and the pore loop, which incorporates the ion selectivity filter (SF) and therefore controls permeation and ion selectivity ***(Figure 2).*** The SF is vital

for the high K+ selectivity and is composed of „signature sequence" T-X-G-Y(F)-G, which is highly conserved across all K+ selective ion channels.

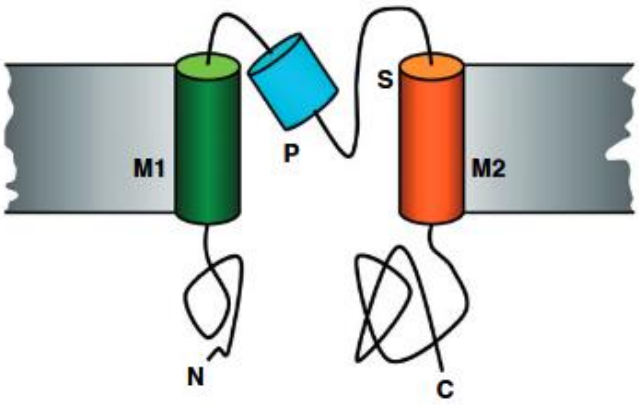

Figure 2: **Topology of the TMD of one Kir subunit**. The TMD is characterized by a conserved structure, two putative membrane-spanning segments (M1 and M2), and a pore-forming P-loop accompanied by a signature sequence (S). ***(Source: Xie, L. H., John, S. A., Ribalet, B., & Weiss, J. N. (2007). Activation of inwardly rectifying potassium (Kir) channels by phosphatidylinositol-4,5-bisphosphate (PIP2): interaction with other regulatory ligands. Progress in biophysics and molecular biology, 94(3), 320–335. https://doi.org/10.1016/j.pbiomolbio.2006.04.001).***

A second building block of Kir channels is an extensive cytoplasmic domain (CTD), that folds into three β sheets. The CTD is composed of the amino (N)- and a carboxy (C) termini, whereas the N-terminus is linked to the TM1 and the C-terminus is linked to TM2. Kir channels contain two gating regions that control ion flix by extending and dilating the ion permeation pathway. The helix-bundle crossing (HBC) gate is located at the TMD, while the narrow G-loop sits at the apex of the CTD ***(Nichols & Lee, 2018; Xie, 2007; Zangerl-Plessl et al., 2019)***.

In the voltage-gated K+ channel (Kv), TM5 and TM6 are analog to TM1 and TM2 in Kir channels as they comprise the channel pore ***(Figure 3)***. Unlike Kir channels, Kv channels consist of six transmembrane helices (TM1-TM6), with helices 1-4 forming the voltage sensor domain (VSD) that underlies the regulation mechanism by membrane voltage ***(Kim & Nimigean,2016).***

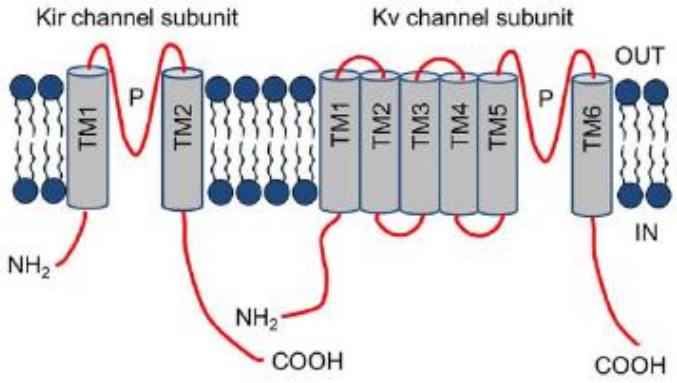

Figure 3: Structural Comparison of Kir and Kv Channel α Subunits. This schematic illustrates the primary structures of the Kir and Kv channel α subunits. Both subunits contain transmembrane domains (TMs), a pore-forming loop (P), and cytosolic N- and C-termini. The Kir subunit consists of two transmembrane segments (TM1, TM2), while the Kv subunit contains six (TM1–TM6) ***(Source: Walsh K. B. (2020). Screening Technologies for Inward Rectifier Potassium Channels: Discovery of New Blockers and Activators. SLAS discovery: advancing life sciences R & D, 25(5), 420–433. https://doi.org/10.1177/2472555220905558).***

1.1.3 Inward rectification

Due to the lack of a VSD, Kir channels are not part of the voltage-gated K+ channel family. Their activity depends on the electrochemical K+ gradient, which is a combination of the K+ concentration gradient and the electrical potential. Under physiological conditions, meaning low extracellular (5 mM) and high intracellular (140 mM) K+ concentrations the resting membrane potential of a neuron (Em ~ - 70mV) is positive to the equilibrium potential of K+ (Ek ~ - 95 mV). Under these physiological conditions, the electrical field gradient is not sufficient enough to balance the concentration gradient, thus resulting in a small K+ outward flux. On the contrary, at Em negative to Ek, there will be a larger inward flux, since the stronger electrical field will tend to draw more K+ into the cell. As a consequence, small depolarizations will cause outward currents, while small hyperpolarization will induce inward Kir currents. It is apparent that, Kir channels play an important role in the maintenance of resting membrane potential ***(Yi & Jan, 2002; Hibino et al., 2010; Walsh, 2020)***.

Inward rectification of Kir channels is gated in a voltage-dependent manner by intracellular substances such as magnesium (Mg2+) and organic polyamines, that

bind in the channel pore and, as a result, block the outward K+ flux under physiological conditions, i.e. at potentials positive to Ek. On the contrary, at voltages negative to Ek, these blockers are displaced from the pore, permitting inward conduction of K+.

The cloning of Kir1.1 and Kir2.1 in 1993 and later all Kir channel subfamilies led to the discovery that specific residues are involved in the rectification of Kir channels. The intensity of rectification depends on the presence of negatively charged residues, such as aspartate (D172 in Kir2.1), glutamate (E), at the lining of the pore. These residues are described as the „rectification controller" and are located at the center of the inner cavity, between the SF and the HBC, where they create a ring of negative charges with which the polyamines can interact ***(Kharade et al., 2017; Nichols & Lee, 2018; Baronas & Kurata,2014).*** Different Kir families experience varying degrees of inward rectification. Kir2.x and Kir3.x are strong inward rectifiers, while Kir1.1 and Kir6.x exhibit weak rectification. Kir4.x channels are classified as intermediately rectifying Kir channels **(*Hibino et al., 2010, Glaaser & Slesinger, 2015)***.

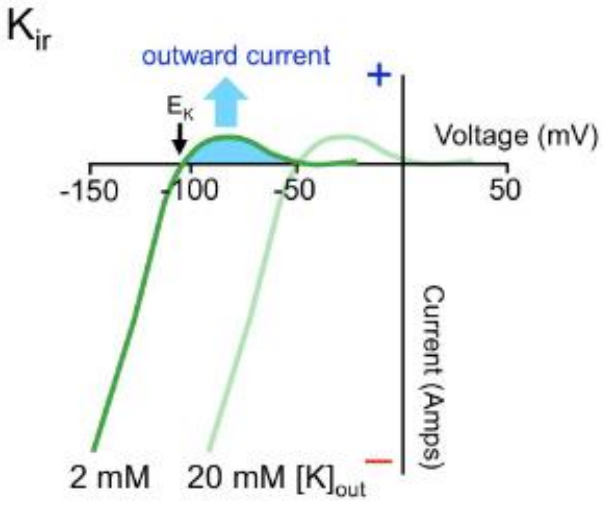

Figure 4: Inward Rectification of Kir Channels. The current-voltage relationship shows that Kir channels conduct inward K+ currents at potentials negative to Ek while outward K+ currents at potentials positive to Ek are blocked. Increasing extracellular K+ concentration shifts the channel's gating behavior ***(Source: Adelman J.P., Clapham D.E., Hibino H., Inanobe A., Jan L.Y., Karschin A., Kubo Y., Kurachi Y., Lazdunski M., Miki T., Nichols C.G., Palmer L.G., Pearson W.L., Sackin H., Seino S., Slesinger P.A., Tucker S. and Vandenberg C.A., (2023). Inwardly rectifying potassium channels (K_{IR}) in GtoPdb v.2023.1. IUPHAR/BPS Guide to Pharmacology CITE, 2023(1). Available from: https://doi.org/10.2218/gtopdb/F74/2023.1).***

1.2 GIRK channel

G protein-gated inwardly rectifying potassium channels (GIRK, Kir3.x), are unique among the Kir channel families since they are activated by G proteins, which are released through stimulation of G protein-coupled receptors (GCPRs) **(*Glaaser & Slesinger,2015)***. GIRK channels are mainly expressed in the heart and the brain, where they regulate the electrical excitability in a variety of distinct cells in the muscle and nerve. They are key players in the generation of slow inhibitory postsynaptic potentials in neurons and the suppression of hormone release in endocrine cells **(*Kurachi & Ishii, 2004)***. Aberrant GIRK channel function is linked to pathophysiological alterations such as epilepsy, Down's syndrome, Parkinson's disease and addiction, making them essential targets for pharmacological intervention in neurological diseases. Research on GIRK-knockout mice reveals the critical role of GIRK2, one of the four GIRK subfamilies (GIRK1-4), in generating neuronal GIRK currents. If GIRK2 channels are absent in mice, they show little to no GIRK current in various areas of the brain ***(Lüscher & Slesinger,2010)***. Given its important role in maintaining neuronal function, GIRK2 will be the focus of this thesis.

1.2.1 Structure

The GIRK channel family comprises of four subfamilies, termed as GIRK1- GIRK4. These channels are also referred to as Kir3.x, where x represents the subunit number from 1 to 4. Similar to other Kirs, GIRK channels can assemble into homomeric or heteromeric configurations, with the subunit composition varying among different cell types and tissues. In neuronal tissues such as the brain GIRK1, GIRK2 and GIRK3 subunits come together to form tetrameric structures. GIRK1 and GIRK3 subunits are always assembling to heterotetramers, while GIRK2 is capable of functioning in homomeric compositions **(Figure 5)**. GIRK2 can be further categorized into GIRK2a, GIRK2b and GIRK2c, as it possesses three splice variants, that vary in the length of the C-terminal domain. In addition to GIRK2, the isoform GIRK4 can also form homomeric structures; however, its expression in the brain is relatively low ***(Lüscher & Slesinger,2010; Hibino et al., 2010)***.

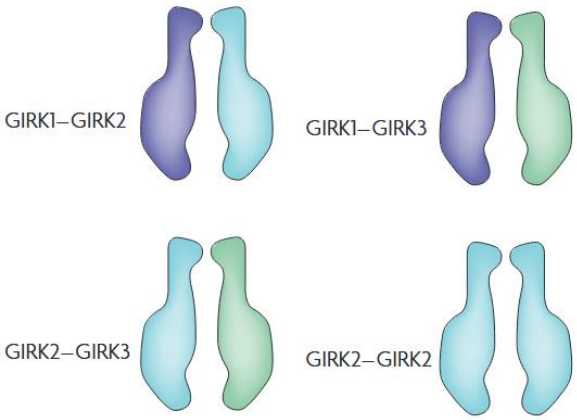

Figure 5: **GIRK Subunit Compositions**. This figure displays the primary GIRK subunit assemblies in neuronal tissues, including three heterotetramers (GIRK1–GIRK2, GIRK1–GIRK3, and GIRK2–GIRK3) and one homotetramer (GIRK2–GIRK2). Each subunit is represented by different colors to distinguish between the various combinations. ***(Source: Lüscher, C., & Slesinger, P. A. (2010). Emerging roles for G protein-gated inwardly rectifying potassium (GIRK) channels in health and disease. Nature reviews. Neuroscience, 11(5), 301–315. https://doi.org/10.1038/nrn2834D).***

The first structure of GIRK2 channel homotetramer, published by Whorton and Mackinnon displays the channel in association with the activator phosphatidylinositol 4,5-bisphosphate (PIP2) ***(Whorton & MacKinnon, 2011)***. Later in 2013, the GIRK2 homotetramer bound to PIP2, Na+ and Gβγ (in PDB: 4KFM), offered valuable insights into the function and regulatory mechanism of GIRK2 channels ***(Whorton & MacKinnon, 2013).***

Figure 6 shows the overall structure of GIRK2 in complex with its regulators Gβγ, PIP2 and Na+. In Chapter 1.1.2, the general structure of Kir channels was described, highlighting the common features this family shares. This chapter will emphasize that, although GIRK exhibits a unique regulatory mechanism, through the involvement of G proteins, notable similarities exist in the overall architecture between GIRK and other Kir channels. They share the fundamental design, including the TMD that comprises the selectivity filter (SF) establishing the high K+ selectivity, and the CTD that plays a crucial role in mediating regulatory interactions ***(Glaaser & Slesinger,2015).***

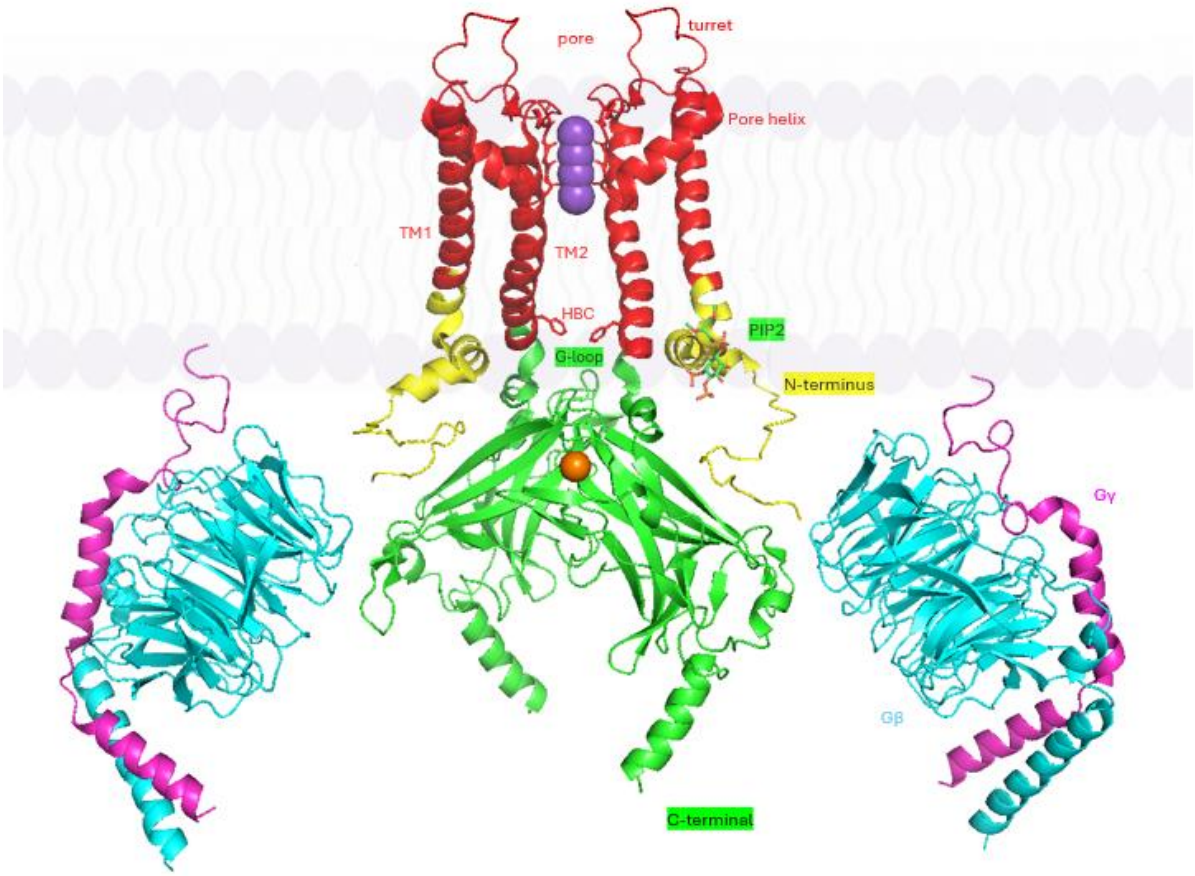

Figure 6. Overall Structure of the GIRK2 bound to its activators Gβγ, PIP2 and Na+. Two opposing GIRK2 subunits, each bound a Gβγ dimer, are shown. The approximate extent of the lipid bilayer is depicted schematically. Transmembrane domains TM1 and TM2, along with the HBC gate, are highlighted in red, with the HBC gate residue F192 shown in stick representation. The N-terminus region is colored yellow, while the CTD and G-loop gate are shown in green. Gβ is displayed in turquoise, and Gγ in magenta. Na+ ions are depicted as orange spheres, and the four K+ ions located in the selectivity filter (SF) are represented as purple spheres. PIP2 is shown in stick representation, colored in green.

1.2.1.1 Transmembrane Domain

The TMD is composed of the two transmembrane helices TM1 and TM2, which are the outer helix in contact with the membrane bilayer and the pore-lining inner helix, respectively. The outer helix accommodates many positively charged residues, which make up the PIP2 binding site by coordinating the negatively charged inositol head group of PIP2. The inner helix harbors one of the two gates for ion conduction, featuring a phenylalanine residue at position 192 (F192). In the homotetrameric GIRK2, four F192 residues come together to form a hydrophobic barrier termed helix bundle crossing gate (HBC). TM1 and TM2 are connected by an extracellular- loop, known as the turret region, a pore helix and the SF. Different to other Kir channels, the GIRK2 turret forms a wider, more open cavity and therefore allows toxin binding such as the binding of tertiapin. The pore helix, positioned behind the SF, plays an essential role in controlling ion passage, and mutations in this region have been shown to alter the channel's selectivity ***(Whorton & MacKinnon, 2011; Whorton & MacKinnon, 2013; Nichols & Lee, 2018; Chen et al., 2019).*** Connected to the inner helix, a reentrant P-loop (Pore-loop) forms the SF, that establishes a narrow path separating the extracellular solution from the inner cavity ***(Hibino et al.,2010)***. The SF consists of a highly conserved amino acid sequence, T-I-G-Y-G, and is essential for selecting K+ over Na+ and other ions. The backbone oxygens of the SF sequence residues create five evenly spaced K+ binding sites. Mutations in the SF cause abnormal SF dynamics and alter the geometry of the filter, which in turn affects the selectivity and conductivity of the channel **(*Friesacher et al., 2022)***. The P-loops of the SF transition into the inner helix, which then extends into the CTD ***(Li et al.,2020).***

1.2.1.2 Cytoplasmic Domain

At the apex of the CTD lies the second regulatory site, called the G-loop gate, which is formed by hydrophobic residues on the βH-βI loop. This site is integrated into the core elements of the CTD, which consists of 14 β strands and two α helices. The β sheets can be further categorized into substructures (βA-βN) with βH and βI constituting part of three loop forming functional units. Other elements, such as the βL-βM

loop, play a crucial role in Gβγ binding. PIP2 binding induces movement in this loop, reconfiguring the surface of the CTD and enhancing its interaction with Gβγ ***(Nguyen et al., 2024; Pegan et al., 2005).***

1.2.2 Regulation

GIRK channels are regulated by G proteins, which are heterotetramers composed of - α, β, and γ subunits and are part of the G protein-coupled receptors (GPCRs) signaling cascade. GPCRs are activated by binding of an agonist, such as acetylcholine (Ach), adenosine, serotonin, dopamine, gamma-aminobutyric acid (GABA), and enkephalin. This triggers the association of a G protein and the exchange of GDP for GTP on the Gα subunit, causing the dissociation of Gα subunit from the Gβγ complex. The released Gβγ then binds to the cytosolic domain (CTD) of the GIRK channel, inducing its transition to the open, active state ***(Dascal & Kahanovitch, 2015)***. The role of Gα in GIRK channel regulation is a topic of ongoing debate, particularly concerning whether Gα plays a purely supportive role in releasing Gβγ or if it exerts additional regulatory functions on the channel. The GTP-bound form of Gα is believed to have no direct effect on GIRK2 channel activation, as it does not activate the channel via Gβγ. In contrast, the GDP-bound form of Gα has been shown to inhibit GIRK2 by promoting the dissociation of Gβγ from the channel **(*Wang et al., 2014)***.

In addition to Gβγ binding to the CTD, another crucial element required for the open channel state is the signaling lipid PIP2. Only when both Gβγ and PIP2 are bound simultaneously does full activation of GIRK2 occur. As previously discussed, the K+ permeation pathway harbors three constriction cites: the SF, HBC gate, and G-loop gate. Studies indicate that G proteins alone primarily open the G-loop gate, but when PIP2 is also present, it induces a rotation of the CTD relative to the TMD, leading to the opening of the HBC gate as well ***(Whorton & MacKinnon, 2011)***. For the HBC gate to open sufficiently to allow passage of hydrated K+ ions, four PIP2 molecules must attach to each subunit ***(Wang et al., 2014; Whorton & MacKinnon, 2011)***. These PIP2 molecules interact with positively charged residues mainly located on the outer helix and the TMD-CTD, thereby promoting the structural changes required for gate opening. This structural alteration of the CTD involves a transition

from the “extended” to the “docked” conformation. Through electrostatic interactions between PIP2 and GIRK, the CTD and TMD are drawn closer together, thereby priming GIRK for Gβγ binding to the CTD ***(Niu et al., 2020).***

Another physiological modulator of GIRK2 activity is intracellular Na+, which acts as an allosteric activator by interacting with the CTD. During depolarization, the intracellular Na+ concentration increases, enhancing the channel's affinity for Gβγ and strengthening its binding to PIP2 ***(Li et al., 2019).*** The regulatory binding site for Na+ is thought to reside in the βC-βD loop of the CTD, specifically at a negatively charged aspartic acid residue (D228) ***(Whorton & MacKinnon, 2011)***. Although Gβγ is the obligatory factor for channel activation, Na+, while not essential, enhances this process. This synergy between Gβγ and Na+ allows for more efficient channel activation and serves as a key mechanism for regulating membrane potential and fine-tuning the cell's inhibitory signaling **(*Li et al., 2019).***

The channel-gating regulatory mechanisms of GIRK2 have been elucidated through high-resolution structures, leading to the proposal of multiple gating hypotheses. Intriguingly, while electrophysiological experiments with GIRK2 in presence of all three physiological regulators - PIP2, Na+, and Gβγ - demonstrate fully active channel states, the crystal structure of GIRK2 bound to these regulators does not capture the channel in an open conformation ***(Li et al., 2019; Whorton & MacKinnon, 2013).*** Therefore, further investigations need to be made for the coherent understanding of the control in GIRK2 channel gating.

1.3 GIRK in disease

Because of their broad function in cardiac and neural excitability, mutations in GIRK channels are associated with a number of diseases. In general, mutations in GIRK have manifold consequences, including alterations in gating and disturbances in ion selectivity caused by mutations in the selectivity filter (SF). A mutation in the SF signature sequence of GIRK2 has been studied in the weaver mouse model that exhibits neuronal and motor behavioral abnormalities. In this model, the highly conserved glycine residue at position 156 of GIRK2 is mutated to a serine, resulting in a constitutively open channel that is insensitive to G-protein activation and no longer

selective for K+, thereby permitting the permeation of Na+ and Ca2+ ions ***(Navarro et al., 1996; Lüscher & Slesinger,2010).*** The functional effect of the G156S mutations depends on the expression levels of the different GIRK subunits. Low GIRK2wv expression results in heteromeric assembly with GIRK1 subunits leading to a reduced function. LoF mutations in GIRK channels cause a reduction in ion flow, which raises neuronal excitability and may result in seizures, as seen in epilepsy **(*Slesinger et al., 1996; Lüscher & Slesinger,2010)***. High GIRK2 wv expression induces abnormal ion flux including excessive Na+ influx, as shown in a Parkinson's disease model, ultimately leading to cell death. GoF mutations in GIRK channels lead to increased ion currents, amplifying the suppression of neural activity and potentially resulting in arrhythmias and conditions such as Down syndrome ***(Kuß et al., 2019; Lüscher & Slesinger,2010).***

The weaver mouse model carries a KCNJ6 (GIRK2wv) mutation involving the replacement of the single amino acid (G156S) and is characterized by male sterility, ataxia, hyperactivity, tremor, and decreased survivability. Homozygous weaver mice exhibit several characteristics, which are linked to nervous system cell death, particularly in the cerebellar granule cells, Purkinje cells, dopaminergic cells of the substantia nigra, and Sertoli cells in the testes ***(Chen et at., 1997).***

1.3.1 Keppen-Lubinsky syndrome

Keppen-Lubinsky syndrome (KPLBS) is a rare disease caused by dominant mutations in the KCNJ6 gene, first characterized in 2001. By 2015, two additional unrelated individuals had been reported with the condition. All three cases involved mutations in the nucleotide sequence, leading to alterations in the selectivity filter (SF) of the GIRK channel. One individual carries a missense mutation (460G>A), resulting in an amino acid change from G154 to S154, which parallels the G156S mutation observed in the weaver mouse model. The other two individuals harbor a three-nucleotide deletion (455_457del), resulting in the loss of threonine at position 152. Although these individuals exhibited different phenotypes in early childhood, they share several clinical similarities, including severe developmental delay, intellectual

disability, hypertonia, and progressive growth impairment. Common physical characteristics include microcephaly, prominent eyes, a narrow nasal bridge, a tented upper lip with an open mouth, an aged appearance, and generalized lipodystrophy ***(Masotti et al., 2015).*** In 2018, another case was reported with a missense mutation (512T>G) in the KCNJ6 gene, resulting in a L171 to R171 substitution. Although this mutation is located behind the selectivity filter (SF) region, several phenotypic similarities were observed. Notably, the patient lacked both the hallmark lipodystrophy and epilepsy seen in other KPLBS cases. However, developmental delay, hypotonia, and a hyperkinetic movement disorder were present, suggesting an expansion of the KPLBS phenotype. Furthermore, the gain-of-function L171R mutation shows similarities to those in the weaver mouse model and KPLBS, causing comparable physiological changes, such as altered G protein activation and ion selectivity ***(Horvath et al., 2018).*** The latest mutation concerning the KCNJ6 gene was found in 2023 when another missense mutation was detected. The 460G >T mutation resulted in an amino acid change from G154 to C154 in the highly conserved region of the SF, causing mild symptoms of KLBS. The physical characteristics of this individual included mild dysmorphic features, such as thin nasal bridge and large eyes without having facial lipodystrophy, observed in other KPLBS patients. In contrast to the patients of Horvath et al. and Masotti et al., this patient did not have microcephaly, had only a mildly reduced IQ of 88, and therefore, she was able to graduate from college. Nevertheless, a new KCNJ6-related disorder was identified: the patient had obsessive-compulsive disorder (OCD), and upon exposure to startling stimuli, a compulsive hair tucking movement occurred, leading to a fall to the ground. In conclusion, this phenotype represents the mildest form among *KCNJ6*-related disorders, emphasizing the importance of expanding the spectrum of these disorders ***(van Midden et al., 2023).***

1.3.2 G156S mutation in the mGIRK2wv SF alters channel regulation

So far, no coherent explanation for the exact regulation of GIRK channels has been established, but studies indicate that GIRK2 must first reach a dynamic activated state to become conductive **(*Friesacher et al., 2022; Whorton & MacKinnon, 2013)***. However, it is unclear how Na+, PIP2 and Gβγ influence channel dynamics

to trigger activation. Interestingly, it has been shown that the GIRK2 mutation G156S in the weaver mouse model (mGIRK2wv) that corresponds to the KPLBS mutation G154S in human GIRK2 (hGIRK2$_{G154S}$) causes impaired channel activation by Gβγ ***(Rossi et al., 1998; Rakic et al., 1973; Slesinger et al., 1996)***. The study by Friesacher et al. reveals an allosteric connection between the SF and the Gβγ-binding site by conducting µs-long molecular dynamic (MD) simulation in combination with electrophysiology experiments of wild-type and mutant GIRK2. The MD simulation showed that the mutation introduces changes in the e φ angle distribution of S156 in the mGIRK2wv SF. This rotation is likely a consequence of a hydrogen bond between the S156 side chain and the backbone oxygen of I155, causing carbonyl oxygen atoms of I155 to reorient, away from the SF pore. Additionally, a shifted distribution of the distance between Cα of I155 in opposing mGIRIK2 subunits was observed, with a wider SF conformation in mGIRK2wv. It is suggested that this alteration in geometry underlies the reduced K+ selectivity of the mutant channels seen in the MD simulations and electrophysiology experiments. Subsequently, a functional mode analysis (FMA), was conducted to investigate the dynamics associated with the mutation-induced I155 fluctuations. Prominent movements were identified in the CTD of mGIRK2wv, particularly in residues 247-254, which constitute the Gβγ- binding site. Based on these findings, the authors suggest a novel aspect of GIRK2 regulation characterized by a direct influence of Gβγ- binding on SF dynamics **(*Friesacher et al., 2022).***

2 Objective

The objective of this master's thesis is to investigate allosteric pathways in the wild-type (mGIRK2wt) and weaver GIRK2 (mGIRK2wv) aiming to identify putative coupling mechanisms underlying channel regulation.

3 Material and Methods

3.1 Sturcture and MD simulationn data

The initial structure of the GIRK2 subunit was derived from the crystal structure available as PDB structure 3SYA, resolved at 3.45 Å ***(Whorton & MacKinnon, 2013)***. The project was based on previously calculated molecular dynamics (MD) simulation data of the GIRK2 channel in a POPC membrane in a 90mM KCL and 90mM NaCl as described in **(*Friesacher et al., 2022).*** Microsecond-long MD simulations of both wild-type (mGIRK2wt) and mutant (mGRIK2wv) GIRK2 homotetramer channels were performed under varying electric fields **(Figure 7).**

		Simulation Time (µs)	Electric Field (mV nm^{-1})	K^+ $PE^\dagger$	Na^+ $PE^\dagger$
mGIRK2$_{wt}$	run1	1	60	4	0
	run2	1	60	18	1
	run3	1	60	4	0
	run4	1	40	7	0
	run5	1	40	3	0
	run6	1	40	4	0
	Total	**6**		**40**	**1**
mGIRK2$_{wv}$	run1	3	60	10	4
	run2	1	60	0	0
	run3	1	60	3	0
	run4	2	40	0	0
	run5	1	40	0	0
	run6	1	50	0	0
	Total	**9**		**13**	**4**

† full permeation events (PE) through the SF

Figure 7. Illustration of six runs of mGIRK2wt and mGIRK2wv under different electrical fields. The mGIRK2wt are conducted with one µs-long simulation time, whereas the first run of mGIRK2wv simulation is three µs-long and the fourth is two µs-long. The strength of electric field varies among the runs from 40-60mV nm-1. The table also includes the number of full permeation events through the SF for K+ and Na+ ***(Source: Friesacher, T., Reddy, H. P., Bernsteiner, H., Carlo Combista, J., Shalomov, B., Bera, A. K., Zangerl-Plessl, E. M., Dascal, N., & Stary-Weinzinger, A. (2022). A selectivity filter mutation provides insights into gating regulation of a K$^+$ channel. Communications biology, 5(1), 345. https://doi.org/10.1038/s42003-022-03303-1***).

3.2 gRINN

The software used for the analysis, get Residue Interaction Energies and Networks (gRINN) **(*Serçinoglu & Ozbek, 2018)***, analyzes MD simulation trajectories to identify amino acid residue interactions and their roles in the protein's dynamics, function, and activity. Trajectories are the primary output of an MD simulation, consisting

of thousands of conformations that capture the biomolecular system's behavior over time. Using either an ensemble of conformations (e.g., from an MD simulation) or a single conformation, gRINN calculates pairwise non-bonded interaction energies between amino acid residues, providing detailed information on residue-level interactions. It constructs interaction energy-based Protein Energy Networks (PENs) to pinpoint residues essential for protein dynamics and uncover allosteric pathways. PENs are a type of Protein Structure Network (PSN), where pairwise non-bonded interactions between individual residues define the "strength" of edges connecting residues (nodes) in the network structure. These values are then applied in further analyses, such as identifying the shortest pathways or calculating residue metrics like degree, betweenness centrality and closeness centrality **(*Serçinoglu & Ozbek, 2018).***

3.2.1 Workflow

3.2.1.1 Calculation set up

gRINN was used along with gmx 2016.4 ***(Abraham et al., 2017)*** executable. The protein structure and topology files were obtained from the MD simulation provided by Theres Frieasacher. Trajectory files were stripped of water, ions, and membrane components, and frames were extracted every 1000th step, irrespective of the trajectory length. An overview of the runs is presented in **Figure 7**.

3.2.1.2 View Results

The software provides graphical user interfaces (GUIs) for inspecting the output, which include both visualization and data generation capabilities **(*Serçinoglu & Ozbek, 2018).*** For this analysis, the network analysis tab in gRINN was used to extract data on residue metrics and shortest pathways. Residue metrics were saved and exported as an Excel table for further processing, while specific shortest pathways were manually selected for targeted residues.

3.3 Analysis of angles, hydrogen bonds, and K+ occupancies

Angles, hydrogen bonds and K+ occupancies were analyzed using the GROMACS tools. Xmgrace was used to plot angles, hydrogen bonds and K+ occupancies.

4 Results

To investigate the effects of the G156S mutation on GIRK2, residue metrics and shortest pathways, which play an important role in the protein's allosteric network, were analyzed. As the first step, residue metrics such as betweenness centrality (BC) and closeness centrality (CC) were evaluated and organized in Excel tables to compare the mGIRK2wt and mGIRK2wv variants. As previously mentioned, BC is a residue-based metric in the PEN and quantifies how often a residue appears on the shortest paths between other residues. Residues with high BC scores often play crucial roles in allosteric signaling. Corresponding to BC, CC measures how efficiently a residue can communicate with all other residues in the PEN. A residue that has a high CC score indicates that it can quickly transfer allosteric signals, acting as a key node for communication within the protein structure **(*Serçinoglu & Ozbek, 2018).***

As shown in **Figure 7**, six runs were analyzed for both mGRIK2wv and mGIRK2wt in different electric fields (40-60mV). For both the mutant and wt channel, BC and CC scores were calculated for each of the six runs and each of the four GIRK2 chains (A-D). Both BC and CC scores were ranked for each chain from highest to lowest score, and the top five residues were selected. For each selected residue, an average rank was calculated over all chains and runs. Moreover, the total occurrence of each residue in the top five lists was calculated **(Suppl. Tables 1-4).** We identified the top three residues with the highest BC and CC scores averaged over all runs and chains for mGIRK2wv and mGIRK2wt **(Figure 8)**. For mGIRK2wv, the top three residues with the highest average BC scores, R240, E311 and E315, also exhibited the highest average CC scores. Similarly, the same residues were identified to have the highest average CC scores in mGIRK2wt. The top three mGIRK2wt average BC scores were calculated for R324, E311 and E315. Importantly, E315 and E311 have high average BC and CC scores in both mGIRK2wv and mGIRK2wt highlighting their important role in the protein's allosteric pathway.

a) mGIRK2wv (BC and CC) and **mGIRK2wt** (CC)

b) mGIRK2wt (BC)

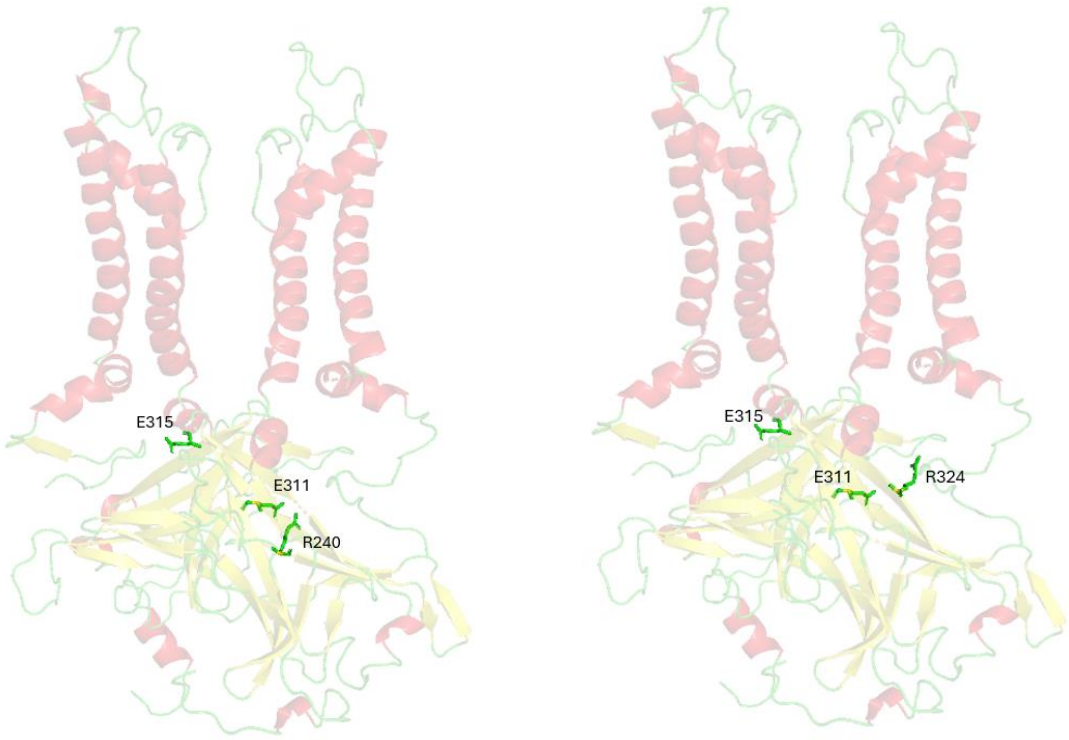

Figure 8: Displays the four residues that had the highest average BC and CC scores from the residue metric analysis. The protein structure is shown as a cartoon representation, with transparency set to 80% for better clarity. Alpha helices are depicted in red, beta sheets in yellow and loops in green. The four residues are shown in stick representation. On the left side are three residues with the highest average BC and CC scores in mGIRK2wv and the highest average CC score in mGIRK2wt, while on the right the three residues with the highest average BC score among the runs in mGIRK2wt are displayed.

In the Supplementary Data, the third column indicates how often a specific residue appears among the top five when ranking residues by BC and CC scores. The total occurrence of amino acids approximately corresponds to their average ranking scores. In order to analyze the effect of mutation on the allosteric network, we probed differences between the BC and CC scores of mGIRK2wv and mGIRK2wt. Residues R272, D271 and D88 showed a decline in occurrence in mGIRK2wv,

whereas M191 showed an increased occurrence. All these residues had a total occurrence greater than six in both mGIRK2wv and mGIRK2wt, meaning that on average they were among the residues with the top five BC and CC scores that appeared more than 25% of the MD-simulation. A representation of these four residues is shown in **Figure 9**.

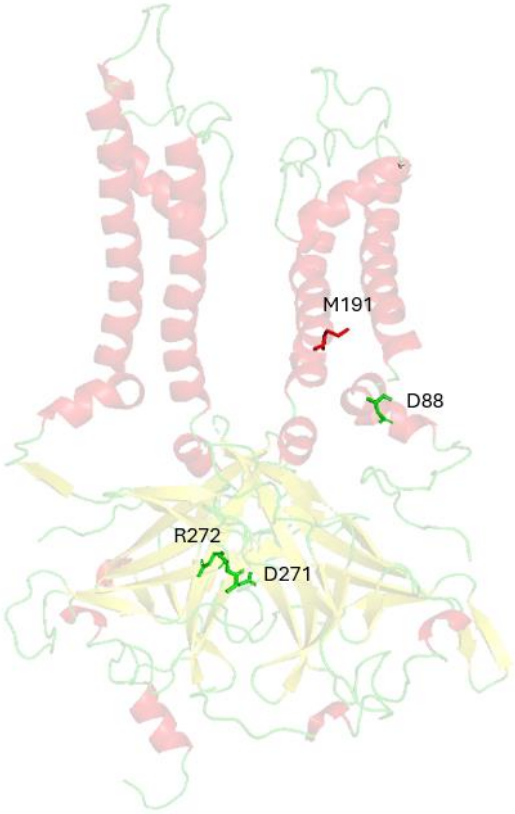

Figure 9: The protein structure is shown as a cartoon representation, with transparency set to 80% for better clarity. Alpha helices are depicted in red, beta sheets in yellow, and loops in green. The four residues are shown in sticks. The three amino acids with decreased total occurrence in mGIRK2wv compared to mGIRK2wt are shown in green, while the residue with increased total occurrence is shown in red.

It was shown that the mutant channel is not activated by Gβγ ***(Rossi et al., 1998; Rakic et al., 1973; Slesinger et al., 1996)***. One possible explanation is that the mutation interferes with the allosteric pathway underlying channel activation by Gβγ ***(Friesacher et al., 2022).*** Therefore, we investigated the shortest pathways between the SF residue S156 and G156 in mGIRK2wv and mGIRK2wt, respectively, and Q248 at the Gβγ- binding site. However, no clear trend or significant differences in the pathways were observed. The tables containing this data are shown in Supplementary Data, **Tables 5 and 6**. Consequently, we examined the shortest pathways between the SF (both S156 and G156 for comparison) and M191, a residue

with increased importance in the mutant **(Figure 9)**. The table analyzing these shortest pathways is shown in the following table **(Table 1)**.

	mGRIK2wv		mGIRK2wt	
run1	chain A**: E150-E152-N184** (Path 1)	intra	chain A: aY157-cL173-cQ176-cI182 (Path 1 wt)	inter
	chain B: Path 1 + C190 (Path 2)	intra		
	chain C: Path 1 + A185 (Path 3)	intra	chain B: Path 3	intra
	chain D: Path 1 + T151 (Path 4)	intra	chain C: Path 3	intra
			chain D: Path 4	intra
run2	chain A: Path 1	intra	chain A: **aY157-cT151-cQ176-cI182** (Path 2 wt)	inter
	chain B: Path 1	intra		
	chain C: Path 3	intra	chain B: Path 2 wt (b-a-a-a)	inter
	chain D: Path 4	intra	chain C: Path 2 wt (c-d-d-d)	inter
			chain D: Path 4	intra
run3	chain A: Path 4	intra	chain A: Path 2 wt	inter
	chain B: Path 2	intra	chain B: Path 2 wt (b-a-a-a)	inter
	chain C: Path 1	intra	chain C: Path 2 wt (c-d-d-d)	inter
	chain D: Path 4	intra	chain D: Path 2 wt (d-b-b-b)	inter
run4	chain A: Path 1	intra	chain A: Path 2 wt	inter
	chain B: Path 3	intra	chain B: Path 3	intra
	chain C: Path 1	intra	chain C: Path 2	intra
	chain D: Path 4	intra	chain D: dI155-bS177-bS181-bI182	inter
run5	chain A: Path 1	intra	chain A: Path 4	intra
	chain B: Path 3	intra	chain B: Path 2 wt (b-a-a-a)	inter
	chain C: I155-T152-Y103-M187	intra	chain C: Path 2	intra
	chain D: Path 4	intra	chain D: Path 1	intra
run6	chain A: Path 4 without E150	intra	chain A: Path 2 wt	inter
	chain B: Path 3	intra	chain B: Path 3	intra
	chain C: Path 1	intra	chain C: Path 3	intra
	chain D: Path 4	intra	chain D: dI155-bS177-bS181-bI182	inter

Table 1 summarizes the shortest pathways from the SF to M191. The first column lists the six runs in mGIRK2wv and mGIRK2wt. The second and third column shows the shortest pathways from S156 to M191 in mGIRK2wv and from G156 to M191 in mGIRK2wt. The residues are represented using the one amino acid code. Four main allosteric paths in the mGIRK2wv, labeled as Path 1–4, are marked the same in mGIRK2wt when shared. Distinct paths in mGIRK2wt are labeled separately, e.g., Path 1 wt. Intra vs. inter behind each row indicates whether the pathway runs within a single subunit or across adjacent subunbunits.

It demonstrates that, in both mGIRK2wv and mGIRK2wt, there are different shortest pathways between the chains. In mGIRK2wv, three common pathways were identified which are all confined to a single subunit (intra). Path 1, S156-E150-E152-N184-M191 appears eight times. Path 3, S156-E150-E152-N184-A185-M191 appears five times. Parth 4, S156-E150-E152-N184-T151-M191 appears seven times, making up 20 out of 24 of most common pathways. In contrast, the shortest pathways in mGIRK2wt vary considerably and run through pairs of adjacent subunits (inter). The most common pathway G156-Y157-T151-Q176-I182-M191 (Path 2 wt in Suppl. **Table 7**) occurs ten times out of 24, making it the most frequent. The second most common pathway G156-E150-E152-N184-A185-M191 appears five out of 24 times and corresponds to Path 3 in mGIRK2wv. The remaining pathways show diverse results. **Figure 10** (a-d) shows a representation of the most common pathways in PyMOL, as it allows for a clear visualization of the shortest pathways between key residues in the protein structure.

a) Path 1 in **mGIRK2wv**

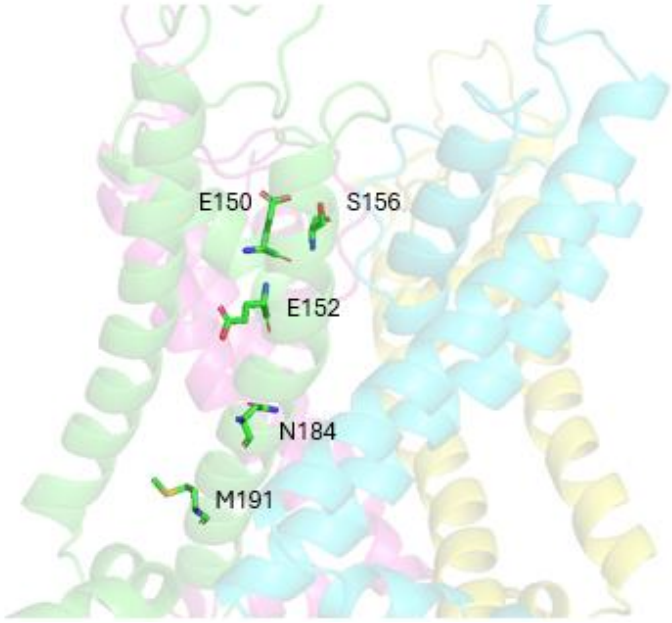

b) Path 3 in **mGIRK2wv** and **mGIRK2wt**

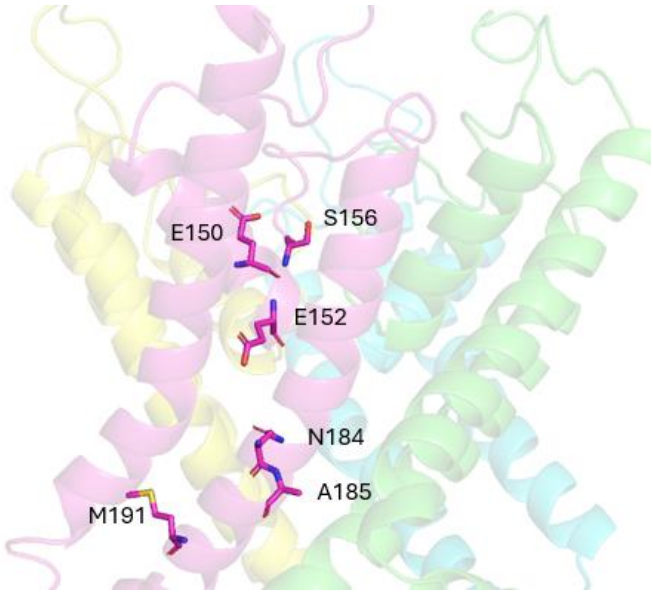

c) Path 4 in **mGIRK2wv**

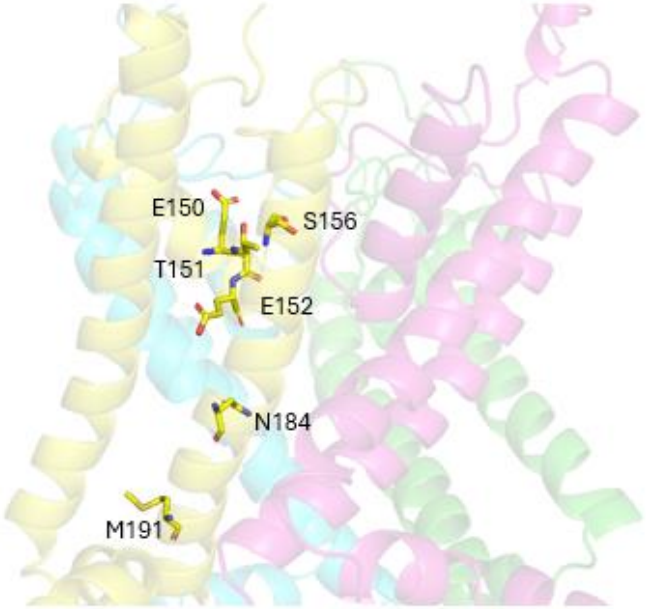

d) Path 2 wt in **mGIRK2wt**

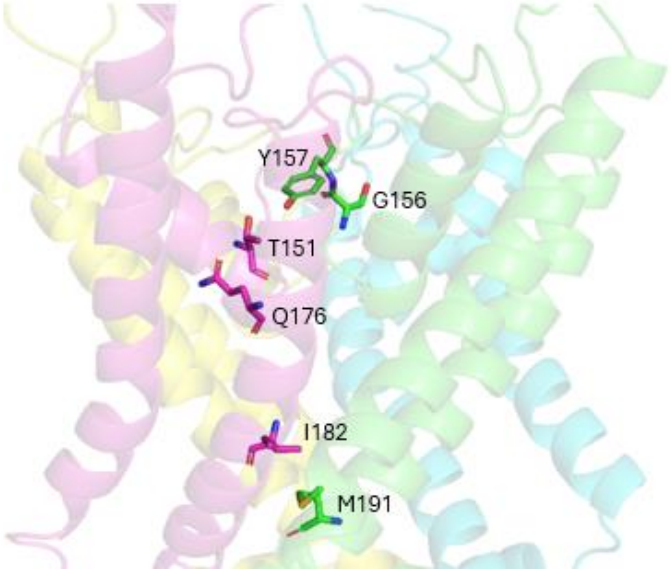

Figure 10 (a-d): represents the shortest pathways from the SF (S156 and G156 in mGIRK2wv and mGIRK2wt, respectively) to M191. The protein backbone is represented in cartoon style and set to a transparency of 80% for a clearer visualization. Chain A is colored in green, chain B in blue, chain C in pink and chain D in yellow. The residues are represented as sticks and contain the same color as the chain they are in. They are marked with the one-letter amino acid code following their position on in the protein sequence.

Further analyses were conducted based on the data obtained here and the findings of Li et al., 2020. Their results indicate that K+ permeation through an open HBC requires a 4-K+ occupancy in the SF-HBC cavity. Their study demonstrated that both E152 and N184 are essential for regulating K+ ion permeation. The negatively charged carboxyl group of E152 induces electrostatic attraction to K+ ions, whereas N184 interacts with K+ through cation-dipole interactions via its carbonyl group. Their results point out the significance of these two residues in K+ permeation through the SF-HBC cavity.

The first analysis involved calculating the angle of E152 in mGIRK2wt and mGIRK2wv, using data obtained from the MD simulation. GROMACS was employed for calculations, and visualization was created with Xmgrace **(Figure 11)**. However, no clear trend could be identified when comparing the angle changes of E152 in mGIRK2wv and mGIRK2wt.

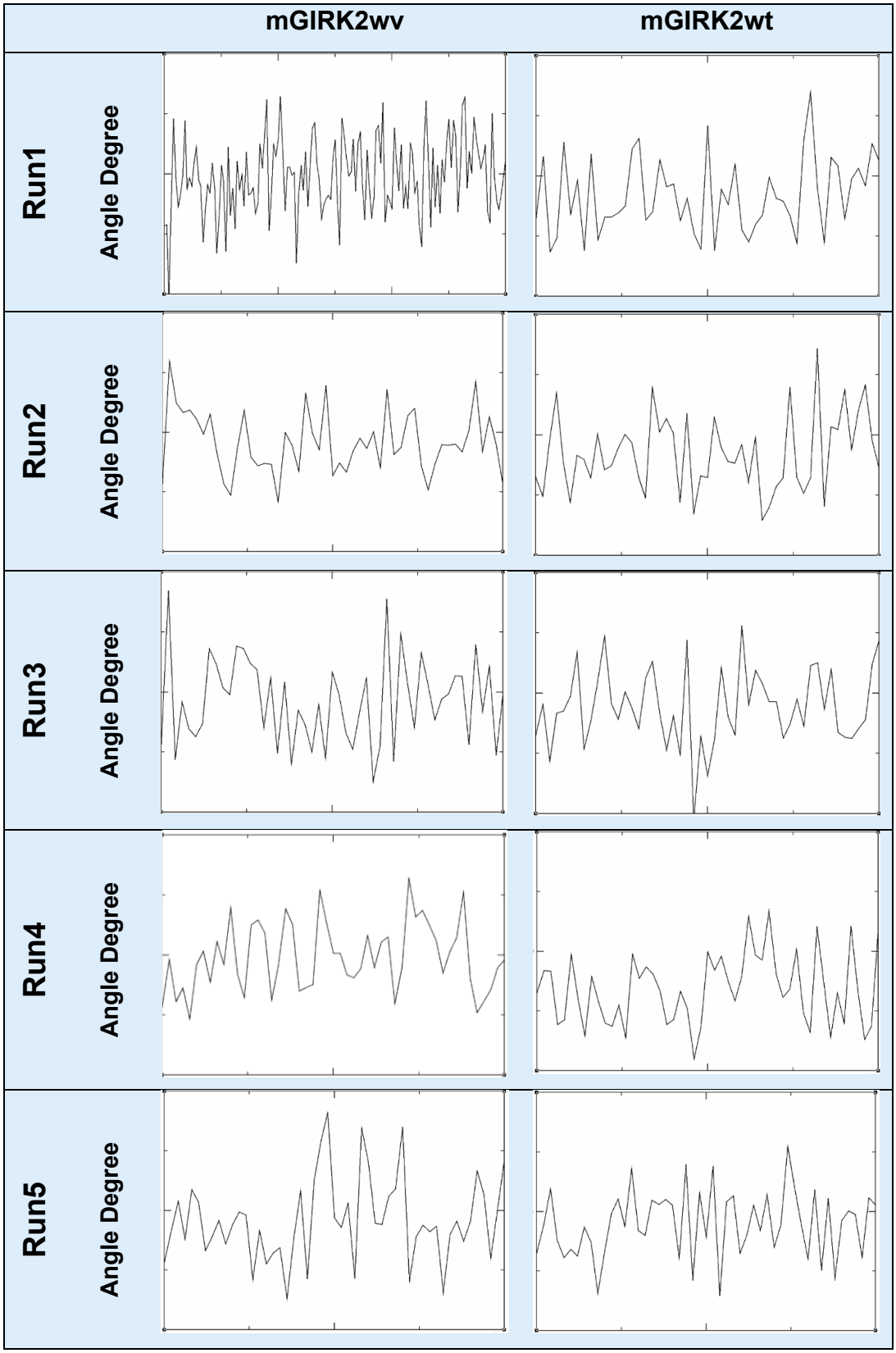
mGIRK2wv
mGIRK2wt
Run1
Angle Degree
Run2
Angle Degree
Run3
Angle Degree
Run4
Angle Degree
Run5
Angle Degree

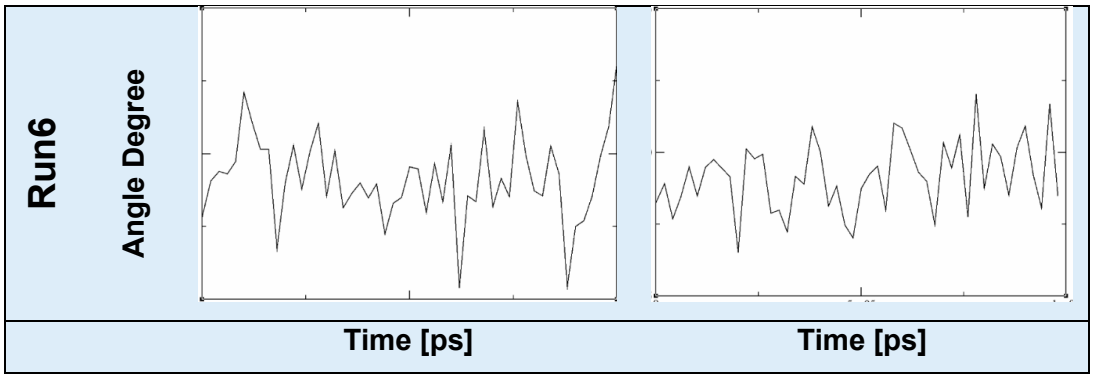

Figure 11: presents time series plots of angle changes of E152, generated using Xmgrace. Both mGIRK2wv and mGIRK2wt were examined in six different runs each, under varying electrical fields (40, 50, 60 mv), for comparison. The Y-axis represents the angle in degrees, while the X-axis denotes time in picoseconds, spanning one microsecond in general. However, in the first figure, the X-axis represents three microseconds.

As stated above, N184, bridging factor between E152 (near SF) and F192 (HBC), plays a crucial role in regulating of K+ ions within the SF-HBC cavity. In a 4-K+ state, a favorable conformation of the carbonyl groups occurs, preventing the formation of cation-dipole interactions with K+ near the HBC gate and thus allowing inward permeation ***(Li et al., 2020)***. Consequently, we monitored the K+ occupancies near N184 in mGIRK2wv and mGIRK2 over time to determine whether the mutation influenced this distribution. The calculation was performed using GROMACS, with the monitored K+ distance from N184 set to 0,7Å **(Figure 12)**. However, no clear trend could be identified when comparing the K+ occupancies near N181 in mGIRK2wv and mGIRK2wt.

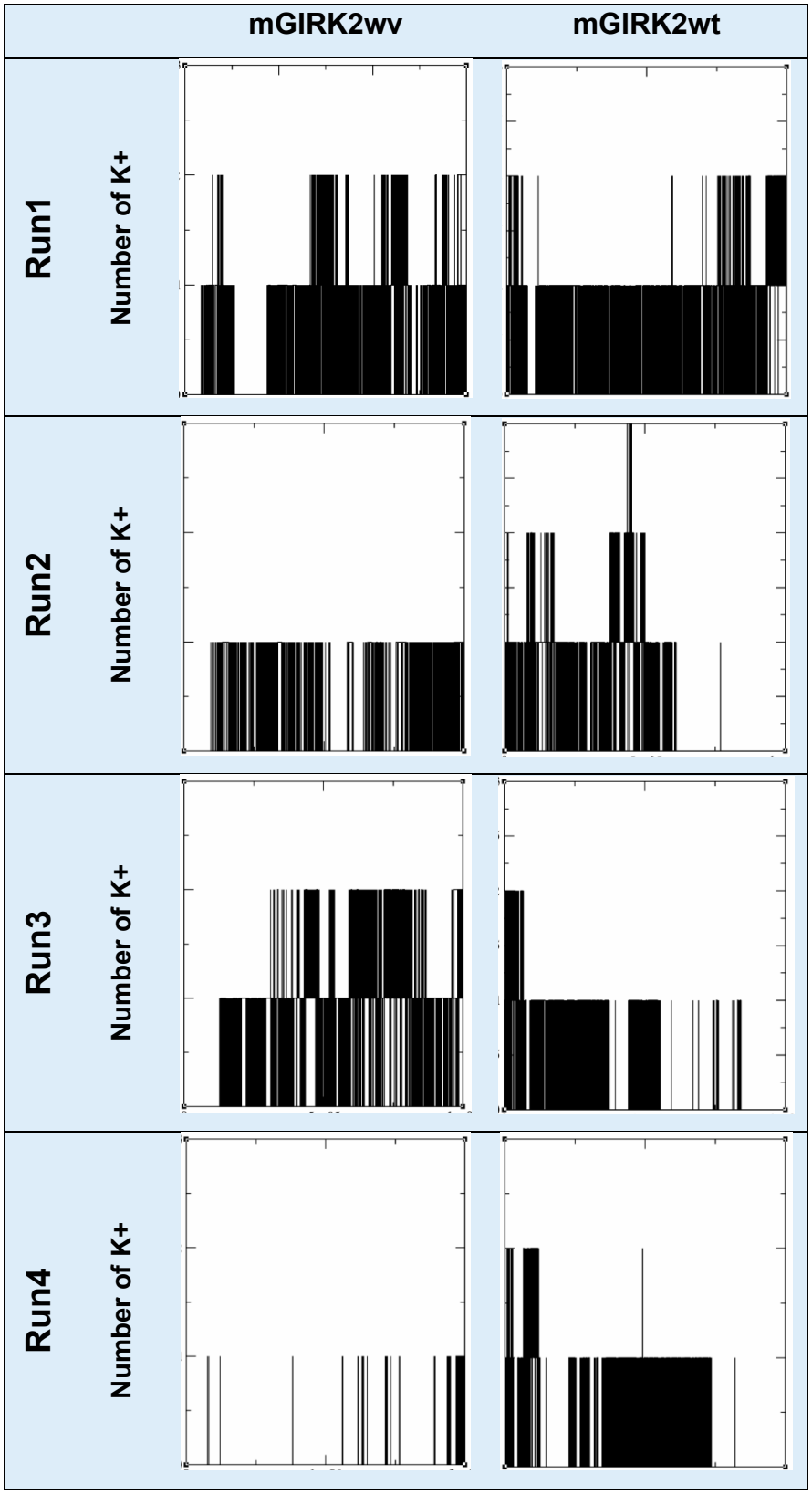
mGIRK2wv
mGIRK2wt
Run1
Number of K+
Run2
Number of K+
Run3
Number of K+
Run4
Number of K+

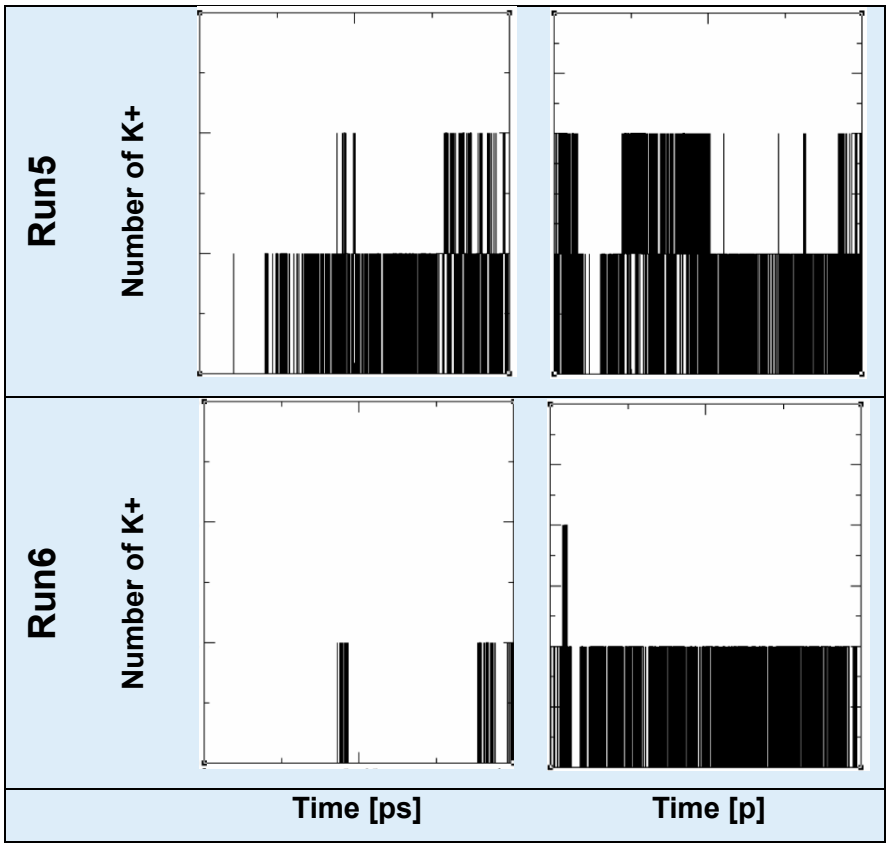

Figure 12: presents time series plots of K+ occupancies within a distance of 0,7Å from N184 over time. Both mGIRK2wv and mGIRK2wt were examined in six different runs each, under varying electrical fields (40, 50, 60 mv), for comparison The Y-Axis represents the number of K+, whereas the X-axis indicates time in picoseconds.

The third analysis involved measuring the distance between E152 and S148, as well as the hydrogen bonds between them over time to determine if the mutation had an impact on these structural features. S148 plays an important role in the allosteric communication of the protein, influencing its interaction with the antiepileptic drug ETX. In GIRK2 it connects residues involved in ETX and Gβ binding ***(Shalomov et al., 2025)***. Both the hydrogen bond analysis and the distance calculation were performed using GROMACS, and the resulting data was plotted as time series in Xmgrace **(Figure 13 and Figure 14)**. However, no clear trend could be identified when either comparing number of hydrogen bonds or comparing the distances between E152 and S148 in mGIRK2wv and mGIRK2wt.

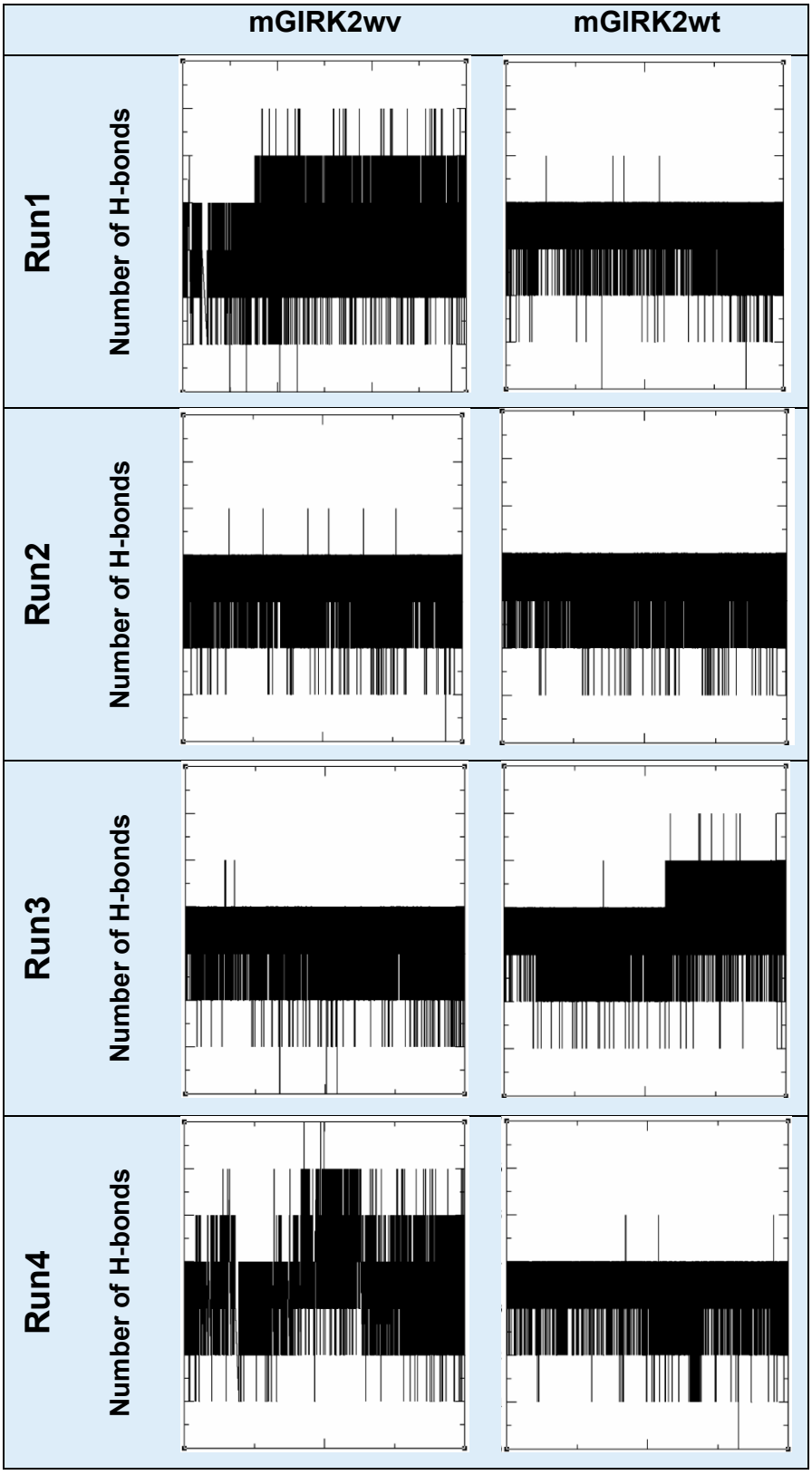
mGIRK2wv
mGIRK2wt
Run1
Number of H-bonds
Run2
Number of H-bonds
Run3
Number of H-bonds
Run4
Number of H-bonds

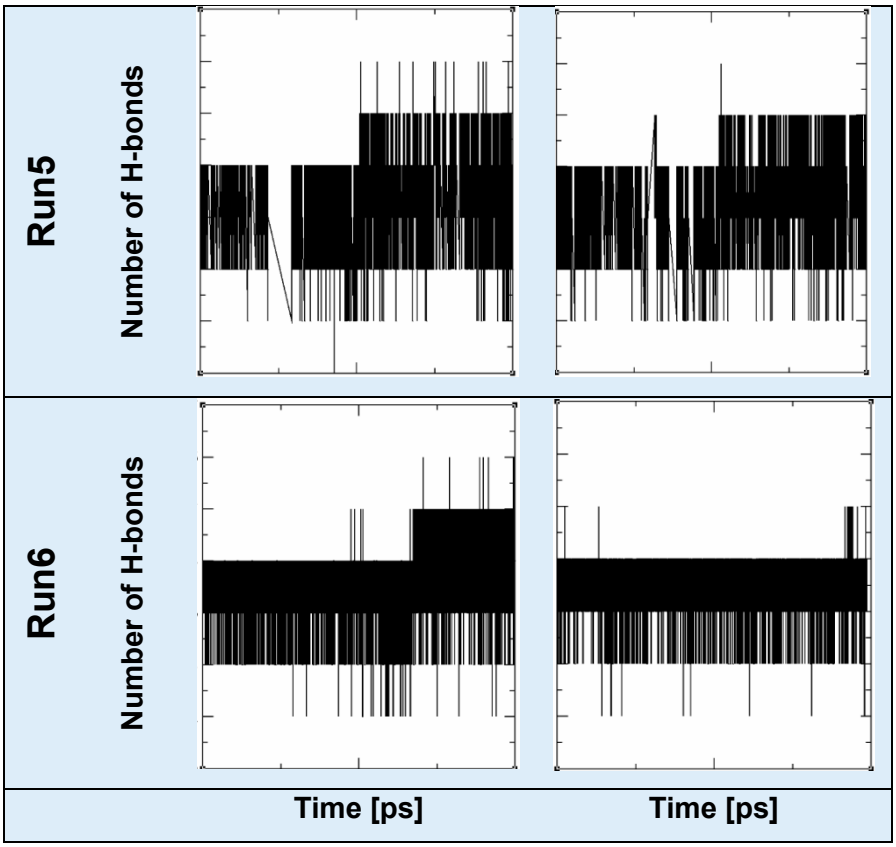

Figure 13: presents time series plots of hydrogen bonds between residues E152 and S148 in over time. Both mGIRK2wv and mGIRK2wt were examined in six different runs each, under varying electrical fields (40, 50, 60 mv), for comparison. The Y-Axis represents the number of hydrogen bonds, whereas the X-axis indicates time in picoseconds.

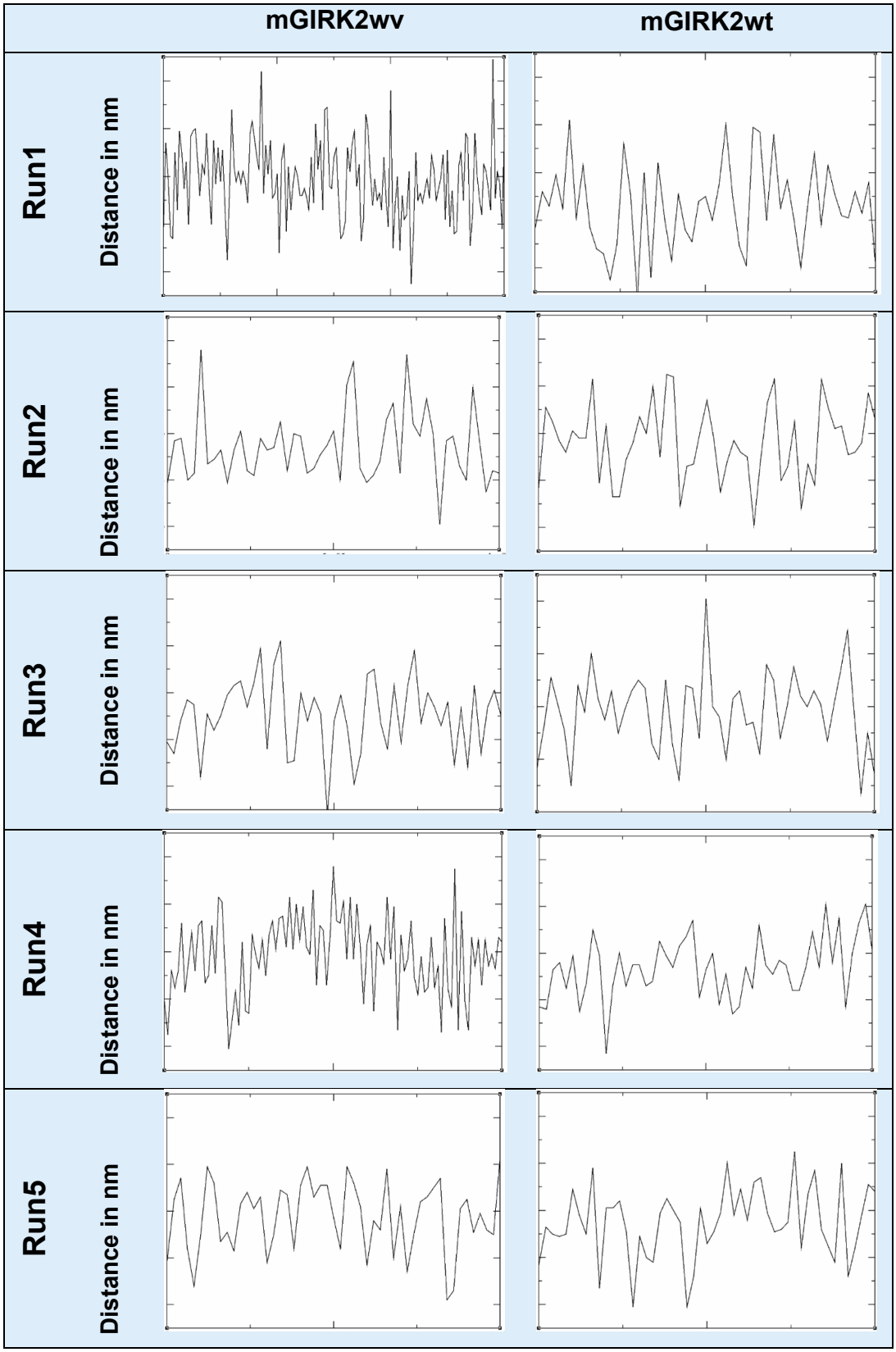
mGIRK2wv
mGIRK2wt
Run1
Distance in nm
Run2
Distance in nm
Run3
Distance in nm
Run4
Distance in nm
Run5
Distance in nm

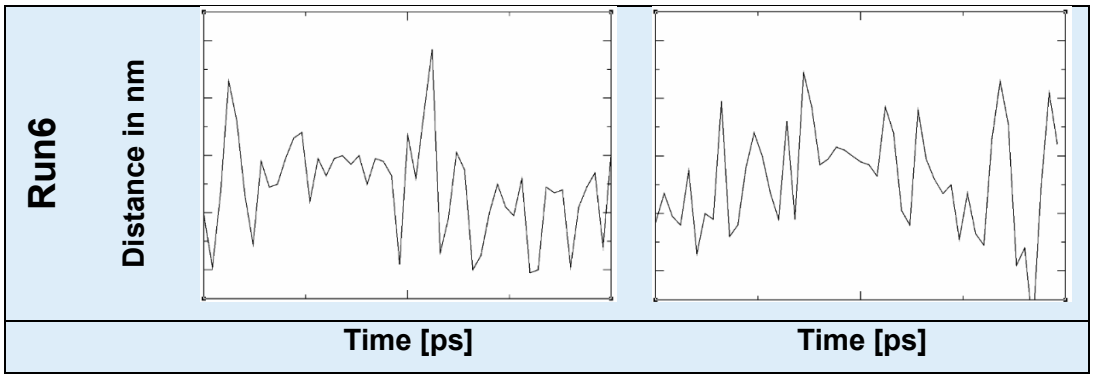

Figures 14: presents time series plots of distances in nm between residues E152 and S148 in over time. Both mGIRK2wv and mGIRK2wt were examined in six different runs each, under varying electrical fields (40, 50, 60 mv), for comparison. The Y-Axis represents the distance in nm, whereas the X-axis indicates time in picoseconds.

5 Discussion

GIRK2 channels are essential mediators of inhibitory neurotransmission in the brain. They are activated by Gβγ, PIP_2, and Na^+. A couple of studies have taken attempts to clarify the underlying mechanism **(*Wang et al., 2014; Whorton & MacKinnon, 2011; Lüscher & Slesinger,2010)*** however the details of the channel regulation by Gβγ, PIP_2, and Na+ remains unclear. The SF mutation (G156S) renders the channels insensitive to Gβγ activation. Investigating the effect of the mutation on GIRK2 using MD simulation, Friesacher et al. proposed a connection between SF and the Gβγ binding site, triggering this aberrant gating behavior. Therefore, we aimed to analyze the allosteric pathways in mGIRK2wv and in mGIRK2wt.

5.1 gRINN analyis

gRINN (get Residue Interaction Energies and Networks) is a tool used to analyze allosteric pathways in protein structures. It calculates pairwise non-bonded interactions and constructs Protein Energy Networks (PENs) to highlight residues essential for allosteric pathways ***(Serçinoglu & Ozbek, 2018).***

5.1.1 Betweenness-and closeness centralities

Betweenness-centrality and closeness-centrality (BC and CC) are both markers that reflect the importance of specific residues in the allosteric signaling of the protein. We identified four residues that might play an important role in GIRK channels allosteric communication pathway, however no clear difference was observed when comparing BC and CC scores of mGIRK2wv and mGIRK2wt

The results indicated that R240, E311 and E315 were the most critical residues associated with the highest BC and CC scores in mGIRK2wv, as well as the highest CC scores in mGIRK2wt. The average BC scores in mGIRK2wt differed only by one residue, R324 ranked among the top three.

R240, E311, E315 and R324 are located in the CTD and have been shown to play important roles in GIRK channel function. E311 is located at the surface of the CTD in (βI-sheet 4KFM: 305–314), a region crucial for Gα binding ***(Ivanina et al., 2004; Clancy et al., 2005).*** Clancy et al. demonstrates that the region between E311 and G335 in GIRK2 is essential for Gα-GTP binding. However, the role of Gα binding for

GIRK activation is enigmatic. Furthermore, a sequence alignment of GIRK1–4 showed that E311, E315, and R324 are identical among the four subfamilies underpinning a potential significance of these residues for channel function. E311, E315, and R324 are located near residues conserved in all GIRK channels such as G318, C321 and A323. Mutation of these residues caused a reduction in Gα-GTP binding to GIRK2.

Another study by Chen et al. highlighted the role of E315 in GIRK channel inward rectification. E315 (located βI-βJ loop in 4KFM: 314-320) is a constriction site for K+ permeation. They show that the E315G mutation leads to a reduction in whole-cell K^+ currents ***(Chen et al., 2002)***. Cui et al. further demonstrated another key function of E315, revealing that this residue plays a crucial role in PIP2 binding to GIRK2 channels. In the apo state (when PIP2 is not bound), E315 forms salt bridges with K199. However, upon PIP2 binding, E315 shifts to interact with R324, (located in the βJ-sheet 4KFM: 320-328), leaving K199 available for PIP2 coordination. The same study also suggested a potential role of R240 in GIRK2 channel activation. R240 (located in βD-sheet 4KFM: 234-244) and it forms hydrogen bonds with L273 in the PIP2-bound state, which is proposed to facilitate the opening of the G-loop gate ***(Cui et al., 2024).***

The analysis with gRINN also identified that residues R272, D271 and D88 display a reduced occurrence in mGIRK2wv, whereas the residue M191 shows an increased occurrence in total. R272 and D271 are located in the CTD (βG-βH- loops 4KFM: 262-279). The same study by Cui et al. revealed that in the apo state, R272 builds salt bridges with D271 that demolish upon PIP2 binding. In the bound state it builds stronger salt bridges with E236 ***(Cui et al., 2024).*** D88 is located in the outer helix of the TMD (TM1) near the PIP2 binding site. However, little has been reported on its role in channel activity. M191 is positioned in the inner helix of the TMD (TM2) near the HBC gate. In Kir1.1 a lysin at the corresponding site (K80) has been identified as a pH sensor, playing a crucial role in channel gating. This study suggests an allosteric link between K80 and the HBC gate residues L161, which occludes the permeation pathway under acidic conditions ***(Hibino et al., 2010).***

5.1.2 Shortest pathways

Allostery is a crucial principle underlying the basic activation mechanism of many channels. Several coupling mechanisms between activator binding sites and the gating regions have also been proposed to underlie GIRK2 regulation ***(Whorton & MacKinnon, 2011; Whorton & MacKinnon, 2013; Bernsteiner et al., 2019; Li et al., 2019; Li et al., 2020; Wang et al., 2014)***. In PENs, the shortest pathways between nodes provide information about residues tightly coupled by their non-bonded interactions and therefore putative allosteric mechanism. We performed shortest pathway analysis with gRINN between SF residue S156 and G156 in mGIRK2wv and mGIRK2wt, respectively, and M191, which shows increased importance in the residue network of mGIRK2wv. This finding shows that the shortest pathways between the chains differ in mGIRK2wv and mGIRK2wt. In mGIRK2wv the most frequently observed pathways were Path 1, S156-E150-E152-N184-M191; Path 3, S156-E150-E152-N184-A185-M191 and Path 4, S156-E150-E152-N184-T151-M191, appearing eight, five and seven times out of 24 pathways, respectively. In mGIRK2wv all pathways are restricted to a single chain, whereas in mGIRk2wt pathways were more variable and predominantly involved adjacent subunit pairs. In mGIRK2wt the most observed pathway was Path 2 wt, G156-Y157-T151-Q176-I182-M191, appearing 10 out of 24 times. The other most frequent pathway corresponded to Path 3 in mGIRK2wv, G156-E150-E152-N184-A185-M191 appeared 5 times. This result in mGIRK2wt. shows cooperation between adjacent subunits that is essential for GIRK channel function and reveals how the disease mutant abolishes these inter communication pathways between subunits in mGIRK2wv. This finding could be an explanation of the results by Surmeier et al. and Slesinger et al, that revealed a reduction in heteromultimer GIRK1 and GIRK2wv channels activity ***(Surmeier et al., 1996; Slesinger et al., 199*6**).** They revealed that GIRK2wv homomultimers show impaired K+ selectivity whereas, a co-expression of GIRK2wv and GIRK1 resulted in a reduced inward K+ flux. Therefore, we propose that weakened subunit cooperation between GIRK subunits could result in the aberrant channel activity. Whether this reduced subunit interaction is the reason why, in the 4KFM structure by Whorton & MacKinnon, the GIRK channel is not fully open yet remains a question for further research ***(Whorton & MacKinnon, 2013).*** One possible

method could be single-molecule fluorescence resonance energy transfer (FRET) analysis used in KirBac1.1 in studies by Wang et al**.** After marking specific residues with fluorophores, they were able to examine conformational changes in lipid membrane ***(Wang et al., 2016)*****.** Another study used solid-state nuclear magnetic resonance (SSNMR) to explore the role of lipids in function-structure relationships in KirBac.1.1. They unveil how the K+ current is regulated by lipid dependent protein cooperativity ***(Yekefallah et al., 2024).***

5.2 Analysis of angles, hydrogen bonds, and K+ occupancies

Residues E152 and N184 are both essential for K+ permeation ***(Li et al., 2020).*** Through electrostatic interactions, they allow K+ to pass through an open HBC gate. Both these residues were part of 23 out of 24 pathways in mGIRK2wv, making them crucial in mGIRK2wv allosteric communication. We conducted calculations of angle changes over time in E152 as well as calculation of K+ distribution near N184 in both mGIRK2wv and mGIRK2wt. The graphs show no obvious changes in mGIRK2wv; however, further runs might be required.

S148 plays an important role in GIRK2 allosteric communication ***(Shalomov et al., 2025).*** We analyzed the distance and hydrogen bonds between E152 and S148, to identify the structural changes caused by the mutation. The results show no detectable changes in mGIRK2, however, to draw a more accurate conclusion additional runs might be required.

6 Conclusion

GIRK2 channels play a critical role in controlling neuronal excitability in the brain by mediating inward rectification of K+ ions upon hyperpolarization at membrane potentials more negative than the equilibrium potential (Ek). The SF is crucial for K+ selectivity, where conserved amino acids within this region are essential for maintaining a proper ion conduction and gating properties. Mutations in the SF of GIRK2 channels have manifold consequences. A mutation in the KCNJ6 gene, encoding for GIRK2 have been identified. G154S mutation in humans causes a rare and severe neurological disease called Keppen-Lubinsky syndrome (KPLBS), characterized by a range of symptoms, including developmental delays, seizures, and generalized. A corresponding mutation in the weaver mouse (G156S) has been shown to disrupt the normal channel function, causing it to remain constitutively open, unresponsive to G-protein activation, and allowing non-selective ion permeation. Previous studies revealed an allosteric communication between the SF and Gβγ-binding site combining MD simulation with electrophysiological experiments. Therefore, this study aimed to investigate allosteric pathways underling channel regulations and activity. A software framework called get Residue Interaction Energies and Networks (gRINN) was used to analyze distinguished pathways in mGIRK2wv and mGIRK2wt. Upon betweenness and closeness centrality analysis four important residues, E315, E311, R240 and R324, have been identified to play a central role in the channel's energy network (PEN). Nevertheless, the mutation did not result in a significant modification of the overall network of the channel; yet one residue M191 gained importance. A consequent analysis of the shortest pathway between S156 and M191 revealed interesting results. We discovered inter subunit communications in mGIRK2wt that are absent in mGRIK2wv. Furthermore, a key path was identified in mGIRK2wv with residues E150-E152-N184. Additional studies, including longer molecular dynamics simulations with more runs, are needed to fully understand the precise mechanisms underlying these interactions and their contribution to the pathophysiology of diseases like KPLBS.

7 Supplementary Data

Table 2: BC scores in mGIRK2wv

Residues	Avarage rank	Total occurence
GLU315	4,20	10
GLU311	4,00	14
ARG240	3,40	15
LYS200	3,07	15
ASP271	3,00	1
GLU331	3,00	1
ARG324	3,00	14
MET191	2,70	10
ARG201	2,69	13
ARG272	2,67	6
ARG77	2,33	3
ASP270	2,29	7
ARG216	2,00	1
ASP62	1,50	2
ASP88	1,50	2
ASN184	1,50	2
LYS61	1,33	3
ASP228	1,00	1
Total		120

Table 3: BC scores in mGIRK2wt

Residues	Avarage rank	Total occurence
GLU315	4,18	11
ARG240	3,63	16
ARG324	3,36	14
GLU311	3,35	17
ASP270	3,17	6
ARG201	2,91	11
ARG272	2,73	11
GLU331	2,67	3
ASP88	2,29	7
LYS200	2,27	11
ARG77	2,00	1
MET191	2,00	3
ASP271	1,83	6
ARG216	1,00	1
ASP228	1,00	1
GLU305	1,00	1
Total		120

Table 4. CC scores in mGIRK2wv

Residues	Avarage rank	Total occurence
GLU311	4,04	24
GLU315	3,32	19
ARG240	3,29	17
ARG324	3,00	15
ARG201	2,89	19
ARG272	2,40	10
LYS200	1,57	7
HIS233	1,00	1
GLY312	1,00	1
LYS199	1,00	2
VAL314	1,00	1
ASP88	1,00	1
ASP228	1,00	2
GLU236	1,00	1
Total		120

Table 5: CC scores in mGIRK2wt

Residues	Avarage rank	Total occurence
GLU311	3,95	21
GLU315	3,61	18
ARG240	3,24	17
ARG201	2,93	15
ARG324	2,93	14
ARG272	2,73	11
LYS199	2,00	5
ASP88	1,67	3
ASP271	1,63	8
LYS200	1,33	3
ASP228	1,20	5
Total		120

Tables 2–5 provide a summary of the BC and CC scores. For each run and GIRK2 subunit, residues were ranked by their BC and CC scores. The top five residues were selected and ranks 5-1 assigned with the highest rank assigned to the residue with the highest score. The first column lists the three-letter amino acid code along with the residue index in the protein sequence. The second column presents the average rank of the amino acid, over all runs and chains. The third column displays the total occurrence of the residue among the top five lists.

Table 6: shortest pathway from SF S156 to Q248 at Gβγ binding site in mGIRK2wv.

Residues	Total occurence in %	Total occurence
SER156	8,66	24
GLN248	8,66	24
GLU150	7,94	22
GLU152	6,86	19
LYS245	6,50	18
ASN184	6,50	18
GLU305	6,14	17
ARG324	5,42	15
LYS200	5,42	15
GLU315	5,42	15
MET191	4,33	12
CYS190	2,53	7
THR151	2,53	7
LYS194	1,81	5
ARG225	1,08	3
GLU203	1,08	3
ASP88	1,08	3
ASN94	0,72	2
LEU257	0,72	2
ILE182	0,72	2
GLN176	0,72	2
MET100	0,72	2
GLN259	0,72	2
PHE274	0,72	2
TRP106	0,72	2
GLU253	0,72	2
VAL188	0,72	2
LYS64	0,72	2
VAL206	0,72	2
LYS247	0,72	2
ILE149	0,72	2
ARG57	0,36	1
SER177	0,36	1
LEU275	0,36	1
GLU251	0,36	1
SER246	0,36	1
ASN258	0,36	1
TYR349	0,36	1
ARG60	0,36	1

Table 7: shortest pathway from SF G156 to Q248 at Gβγ binding site in mGIRK2wt.

Residues	Total occurence in %	Total occurence
GLY156	8,45	24
GLN248	8,45	24
GLU305	6,34	18
LYS245	6,34	18
GLU150	6,34	18
ARG324	4,93	14
GLU315	3,87	11
GLU152	3,87	11
LYS200	3,17	9
ASN184	3,17	9
CYS190	2,46	7
LYS194	2,11	6
THR151	2,11	6
TRP106	1,76	5
ILE149	1,76	5
ASP88	1,76	5
ASN94	1,41	4
GLY180	1,41	4
ARG225	1,41	4
ILE195	1,41	4
TYR102	1,41	4
ARG77	1,41	4
TYR157	1,41	4
GLU253	1,41	4
LEU173	1,41	4
PHE186	1,06	3
VAL188	1,06	3
PHE207	1,06	3
ILE182	1,06	3
LYS64	1,06	3
MET100	1,06	3
PHE98	0,70	2
LYS90	0,70	2
GLN176	0,70	2
LEU96	0,70	2
MET191	0,70	2
GLU203	0,70	2
SER181	0,70	2

CYS65	0,36	1
ASP62	0,36	1
SER181	0,36	1
LYS90	0,36	1
ARG77	0,36	1
HIS233	0,36	1
TYR102	0,36	1
HIS68	0,36	1
TYR58	0,36	1
PHE207	0,36	1
LEU96	0,36	1
VAL87	0,36	1
ARG201	0,36	1
ILE155	0,36	1
Total	100	277

ARG57	0,70	2
ILE155	0,70	2
ALA316	0,70	2
HIS233	0,35	1
LYS199	0,35	1
LYS61	0,35	1
ARG60	0,35	1
ASN66	0,35	1
LEU86	0,35	1
ARG201	0,35	1
TYR78	0,35	1
SER246	0,35	1
VAL226	0,35	1
THR153	0,35	1
ILE244	0,35	1
GLN259	0,35	1
PHE274	0,35	1
TYR58	0,35	1
LYS247	0,35	1
SER177	0,35	1
ASP228	0,35	1
LEU179	0,35	1
PHE192	0,35	1
Total	100	284

Tables 6-7 summarize the shortest pathways generated in gRINN. The first column lists the three-letter amino acid code along with the residue's position in the protein sequence. The second column presents the percentage occurrence of the amino acid across all four chains and six runs, totaling 24 cases. The third column shows the sum of occurrences, with 24 being the maximum possible value. Table 5 displays the shortest pathway from SF S156 to Q248 at Gβγ binding site in mGIRK2wv while Table 6 shows the shortest pathway from SF G156 to Q248 at Gβγ binding site in mGIRK2wt.

8 References

1. **Lu Z.** (2004). Mechanism of rectification in inward-rectifier K+ channels. *Annual review of physiology*, *66*, 103–129. https://doi.org/10.1146/annurev.physiol.66.032102.150822
2. **Hibino**, H., Inanobe, A., Furutani, K., Murakami, S., Findlay, I., & Kurachi, Y. (2010). Inwardly rectifying potassium channels: their structure, function, and physiological roles. *Physiological reviews*, *90*(1), 291–366. https://doi.org/10.1152/physrev.00021.2009
3. **Kurata**, H. T., Phillips, L. R., Rose, T., Loussouarn, G., Herlitze, S., Fritzenschaft, H., Enkvetchakul, D., Nichols, C. G., & Baukrowitz, T. (2004). Molecular basis of inward rectification: polyamine interaction sites located by combined channel and ligand mutagenesis. *The Journal of general physiology*, *124*(5), 541–554. https://doi.org/10.1085/jgp.200409159
4. **Hager**, N. A., McAtee, C. K., Lesko, M. A., & O'Donnell, A. F. (2022). Inwardly Rectifying Potassium Channel Kir2.1 and its "Kir-ious" Regulation by Protein Trafficking and Roles in Development and Disease. *Frontiers in cell and developmental biology*, *9*, 796136. https://doi.org/10.3389/fcell.2021.796136
5. **Zangerl-Plessl**, E. M., Qile, M., Bloothooft, M., Stary-Weinzinger, A., & van der Heyden, M. A. G. (2019). Disease Associated Mutations in K_{IR} Proteins Linked to Aberrant Inward Rectifier Channel Trafficking. *Biomolecules*, *9*(11), 650. https://doi.org/10.3390/biom9110650
6. **Zubcevic**, L., Bavro, V. N., Muniz, J. R., Schmidt, M. R., Wang, S., De Zorzi, R., Venien-Bryan, C., Sansom, M. S., Nichols, C. G., & Tucker, S. J. (2014). Control of KirBac3.1 potassium channel gating at the interface between cytoplasmic domains. *The Journal of biological chemistry*, *289*(1), 143–151. https://doi.org/10.1074/jbc.M113.501833
7. **Nichols**, C. G., & Lee, S. J. (2018). Polyamines and potassium channels: A 25-year romance. *The Journal of biological chemistry*, *293*(48), 18779–18788. https://doi.org/10.1074/jbc.TM118.003344
8. **Xie**, L. H., John, S. A., Ribalet, B., & Weiss, J. N. (2007). Activation of inwardly rectifying potassium (Kir) channels by phosphatidylinosital-4,5-bisphosphate (PIP2): interaction with other regulatory ligands. *Progress in biophysics and molecular biology*, *94*(3), 320–335. https://doi.org/10.1016/j.pbiomolbio.2006.04.001
9. **Walsh** K. B. (2020). Screening Technologies for Inward Rectifier Potassium Channels: Discovery of New Blockers and Activators. *SLAS discovery: advancing life sciences R & D*, *25*(5), 420–433. https://doi.org/10.1177/2472555220905558
10. **Kim**, D. M., & Nimigean, C. M. (2016). Voltage-Gated Potassium Channels: A Structural Examination of Selectivity and Gating. *Cold Spring Harbor perspectives in biology*, *8*(5), a029231. https://doi.org/10.1101/cshperspect.a029231
11. B. Alexander **Yi**, Lily Y. **Jan**, Ion Channels, Editor(s): V.S. Ramachandran, Encyclopedia of the Human Brain, Academic Press, 2002, Pages 599-615 ISBN 9780122272103,https://doi.org/10.1016/B0-12-227210-2/00180 (https://www.sciencedirect.com/science/article/pii/B0122272102001801)
12. **Kharade**, S. V., Sheehan, J. H., Figueroa, E. E., Meiler, J., & Denton, J. S. (2017). Pore Polarity and Charge Determine Differential Block of Kir1.1 and Kir7.1 Potassium Channels by Small-Molecule Inhibitor VU590. *Molecular pharmacology*, *92*(3), 338–346. https://doi.org/10.1124/mol.117.108472
13. **Baronas**, V. A., & **Kurata**, H. T. (2014). Inward rectifiers and their regulation by endogenous polyamines. *Frontiers in physiology*, *5*, 325. https://doi.org/10.3389/fphys.2014.00325
14. **Adelman** J.P., Clapham D.E., Hibino H., Inanobe A., Jan L.Y., Karschin A., Kubo Y., Kurachi Y., Lazdunski M., Miki T., Nichols C.G., Palmer L.G., Pearson W.L., Sackin H., Seino S., Slesinger P.A., Tucker S. and Vandenberg C.A., (2023). Inwardly rectifying potassium channels (K_{IR}) in GtoPdb v.2023.1. *IUPHAR/BPS Guide to Pharmacology CITE*, *2023(1)*. Available from: https://doi.org/10.2218/gtopdb/F74/2023.1.
15. **Glaaser**, I. W., & **Slesinger**, P. A. (2015). Structural Insights into GIRK Channel Function. *International review of neurobiology*, *123*, 117–160. https://doi.org/10.1016/bs.irn.2015.05.014
16. **Kurachi**, Y., & **Ishii**, M. (2004). Cell signal control of the G protein-gated potassium channel and its subcellular localization. *The Journal of physiology*, *554*(Pt 2), 285–294. https://doi.org/10.1113/jphysiol.2003.048439

17. **Lüscher**, C., & **Slesinger**, P. A. (2010). Emerging roles for G protein-gated inwardly rectifying potassium (GIRK) channels in health and disease. *Nature reviews. Neuroscience*, *11*(5), 301–315. https://doi.org/10.1038/nrn2834
18. **Whorton**, M. R., & **MacKinnon**, R. (2011). Crystal structure of the mammalian GIRK2 K+ channel and gating regulation by G proteins, PIP2, and sodium. *Cell*, *147*(1), 199–208. https://doi.org/10.1016/j.cell.2011.07.046
19. **Whorton**, M. R., & **MacKinnon**, R. (2013). X-ray structure of the mammalian GIRK2-βγ G-protein complex. *Nature*, *498*(7453), 190–197. https://doi.org/10.1038/nature12241
20. **Chen**, I. S., Liu, C., Tateyama, M., Karbat, I., Uesugi, M., Reuveny, E., & Kubo, Y. (2019). Non-sedating antihistamines block G-protein-gated inwardly rectifying K^+ channels. *British journal of pharmacology*, *176*(17), 3161–3179. https://doi.org/10.1111/bph.14717
21. **Li**, D. L., Hu, L., Wang, L., & Chen, C. L. (2020). Permeation mechanisms through the selectivity filter and the open helix bundle crossing gate of GIRK2. *Computational and structural biotechnology journal*, *18*, 3950–3958. https://doi.org/10.1016/j.csbj.2020.11.039
22. **Friesacher**, T., Reddy, H. P., Bernsteiner, H., Carlo Combista, J., Shalomov, B., Bera, A. K., Zangerl-Plessl, E. M., Dascal, N., & Stary-Weinzinger, A. (2022). A selectivity filter mutation provides insights into gating regulation of a K^+ channel. *Communications biology*, *5*(1), 345. https://doi.org/10.1038/s42003-022-03303-1
23. **Nguyen**, H., Glaaser, I. W., & Slesinger, P. A. (2024). Direct modulation of G protein-gated inwardly rectifying potassium (GIRK) channels. *Frontiers in physiology*, *15*, 1386645. https://doi.org/10.3389/fphys.2024.1386645
24. **Pegan**, S., Arrabit, C., Zhou, W., Kwiatkowski, W., Collins, A., Slesinger, P. A., & Choe, S. (2005). Cytoplasmic domain structures of Kir2.1 and Kir3.1 show sites for modulating gating and rectification. *Nature neuroscience*, *8*(3), 279–287. https://doi.org/10.1038/nn1411
25. **Li**, D., Jin, T., Gazgalis, D., Cui, M., & Logothetis, D. E. (2019). On the mechanism of GIRK2 channel gating by phosphatidylinositol bisphosphate, sodium, and the Gβγ dimer. *The Journal of biological chemistry*, *294*(49), 18934–18948. https://doi.org/10.1074/jbc.RA119.010047
26. **Dascal**, N., & **Kahanovitch**, U. (2015). The Roles of Gβγ and Gα in Gating and Regulation of GIRK Channels. *International review of neurobiology*, *123*, 27–85. https://doi.org/10.1016/bs.irn.2015.06.001
27. **Wang**, W., Whorton, M. R., & MacKinnon, R. (2014). Quantitative analysis of mammalian GIRK2 channel regulation by G proteins, the signaling lipid PIP2 and Na+ in a reconstituted system. *eLife*, *3*, e03671. https://doi.org/10.7554/eLife.03671
28. **Niu**, Y., Tao, X., Touhara, K. K., & MacKinnon, R. (2020). Cryo-EM analysis of PIP_2 regulation in mammalian GIRK channels. *eLife*, *9*, e60552. https://doi.org/10.7554/eLife.60552
29. **Jeremic**, D., Sanchez-Rodriguez, I., Jimenez-Diaz, L., & Navarro-Lopez, J. D. (2021). Therapeutic potential of targeting G protein-gated inwardly rectifying potassium (GIRK) channels in the central nervous system. *Pharmacology & therapeutics*, *223*, 107808. https://doi.org/10.1016/j.pharmthera.2021.107808
30. **Kuß**, J., Stallmeyer, B., Goldstein, M., Rinné, S., Pees, C., Zumhagen, S., Seebohm, G., Decher, N., Pott, L., Kienitz, M. C., & Schulze-Bahr, E. (2019). Familial Sinus Node Disease Caused by a Gain of GIRK (G-Protein Activated Inwardly Rectifying K^+ Channel) Channel Function. *Circulation. Genomic and precision medicine*, *12*(1), e002238. https://doi.org/10.1161/CIRCGEN.118.002238
31. **Slesinger**, P. A., Patil, N., Liao, Y. J., Jan, Y. N., Jan, L. Y., & Cox, D. R. (1996). Functional effects of the mouse weaver mutation on G protein-gated inwardly rectifying K+ channels. *Neuron*, *16*(2), 321–331. https://doi.org/10.1016/s0896-6273(00)80050-1
32. **Chen**, S. C., Ehrhard, P., Goldowitz, D., & Smeyne, R. J. (1997). Developmental expression of the GIRK family of inward rectifying potassium channels: implications for abnormalities in the weaver mutant mouse. *Brain research*, *778*(2), 251–264. https://doi.org/10.1016/s0006-8993(97)00896-2
33. **Navarro**, B., Kennedy, M. E., Velimirovíc, B., Bhat, D., Peterson, A. S., & Clapham, D. E. (1996). Nonselective and G betagamma-insensitive weaver K+ channels. *Science (New York, N.Y.)*, *272*(5270), 1950–1953. https://doi.org/10.1126/science.272.5270.1950
34. **Masotti**, A., Uva, P., Davis-Keppen, L., Basel-Vanagaite, L., Cohen, L., Pisaneschi, E., Celluzzi, A., Bencivenga, P., Fang, M., Tian, M., Xu, X., Cappa, M., & Dallapiccola, B. (2015). Keppen-Lubinsky syndrome is caused

by mutations in the inwardly rectifying K+ channel encoded by KCNJ6. *American journal of human genetics*, *96*(2), 295–300. https://doi.org/10.1016/j.ajhg.2014.12.011

35. **Horvath**, G. A., Zhao, Y., Tarailo-Graovac, M., Boelman, C., Gill, H., Shyr, C., Lee, J., Blydt-Hansen, I., Drögemöller, B. I., Moreland, J., Ross, C. J., Wasserman, W. W., Masotti, A., Slesinger, P. A., & van Karnebeek, C. D. M. (2018). Gain-of-function KCNJ6 Mutation in a Severe Hyperkinetic Movement Disorder Phenotype. *Neuroscience*, *384*, 152–164. https://doi.org/10.1016/j.neuroscience.2018.05.031
36. **Serçinoglu**, O., & **Ozbek**, P. (2018). gRINN: a tool for calculation of residue interaction energies and protein energy network analysis of molecular dynamics simulations. *Nucleic acids research*, *46*(W1), W554–W562. https://doi.org/10.1093/nar/gky381
37. **Shalomov**, B., Friesacher, T., Yakubovich, D., Combista, J. C., Reddy, H. P., Dabbah, S., Bernsteiner, H., Zangerl-Plessl, E. M., Stary-Weinzinger, A., & Dascal, N. (2025). Ethosuximide: Subunit- and Gβγ-dependent blocker and reporter of allosteric changes in GIRK channels. *British journal of pharmacology*, 10.1111/bph.17446. Advance online publication. https://doi.org/10.1111/bph.17446
38. **van Midden**, V. M., Kinsley, L., Fraint, A., Krainc, D., & Mencacci, N. E. (2023). Expanding the spectrum of KCNJ6-related disorders: Milder phenotype with pathological startle responses. *Clinical genetics*, *103*(1), 103–108. https://doi.org/10.1111/cge.14226
39. **Abraham**, **M. J.**, van der Spoel, D., Lindahl, E., Hess, B., & GROMACS development team. (2017). *GROMACS user manual* (Version 2016.4). Retrieved from www.gromacs.org
40. **Rossi**, **P.**, De Filippi, G., Armano, S., Taglietti, V., & D'Angelo, E. (1998). The weaver mutation causes a loss of inward rectifier current regulation in premigratory granule cells of the mouse cerebellum. *The Journal of neuroscience : the official journal of the Society for Neuroscience*, *18*(10), 3537–3547. https://doi.org/10.1523/JNEUROSCI.18-10-03537.1998
41. **Rakic**, **P.**, & Sidman, R. L. (1973). Organization of cerebellar cortex secondary to deficit of granule cells in weaver mutant mice. *The Journal of comparative neurology*, *152*(2), 133–161. https://doi.org/10.1002/cne.901520203
42. **Ivanina**, **T.**, Varon, D., Peleg, S., Rishal, I., Porozov, Y., Dessauer, C. W., Keren-Raifman, T., & Dascal, N. (2004). Galphai1 and Galphai3 differentially interact with, and regulate, the G protein-activated K+ channel. *The Journal of biological chemistry*, *279*(17), 17260–17268. https://doi.org/10.1074/jbc.M313425200
43. **Clancy**, **S. M.**, Fowler, C. E., Finley, M., Suen, K. F., Arrabit, C., Berton, F., Kosaza, T., Casey, P. J., & Slesinger, P. A. (2005). Pertussis-toxin-sensitive Galpha subunits selectively bind to C-terminal domain of neuronal GIRK channels: evidence for a heterotrimeric G-protein-channel complex. Molecular and cellular neurosciences, 28(2), 375–389. https://doi.org/10.1016/j.mcn.2004.10.009
44. **Cui**, **M.**, Lu, Y., Ma, X., & Logothetis, D. E. (2024). Molecular mechanism of GIRK2 channel gating modulated by cholesteryl hemisuccinate. Frontiers in physiology, 15, 1486362. https://doi.org/10.3389/fphys.2024.1486362
45. **Chen**, **L.**, Kawano, T., Bajic, S., Kaziro, Y., Itoh, H., Art, J. J., Nakajima, Y., & Nakajima, S. (2002). A glutamate residue at the C terminus regulates activity of inward rectifier K+ channels: implication for Andersen's syndrome. Proceedings of the National Academy of Sciences of the United States of America, 99(12), 8430–8435. https://doi.org/10.1073/pnas.122682899
46. **Slesinger**, P. A., Patil, N., Liao, Y. J., Jan, Y. N., Jan, L. Y., & Cox, D. R. (1996). Functional effects of the mouse weaver mutation on G protein-gated inwardly rectifying K+ channels. *Neuron*, *16*(2), 321–331. https://doi.org/10.1016/s0896-6273(00)80050-1
47. **Surmeier**, D. J., Mermelstein, P. G., & Goldowitz, D. (1996). The weaver mutation of GIRK2 results in a loss of inwardly rectifying K+ current in cerebellar granule cells. *Proceedings of the National Academy of Sciences of the United States of America*, *93*(20), 11191–11195. https://doi.org/10.1073/pnas.93.20.11191
48. **Wang**, S., Vafabakhsh, R., Borschel, W. F., Ha, T., & Nichols, C. G. (2016). Structural dynamics of potassium-channel gating revealed by single-molecule FRET. *Nature structural & molecular biology*, *23*(1), 31–36. https://doi.org/10.1038/nsmb.3138

49. **Yekefallah**, M., van Aalst, E. J., van Beekveld, R. A. M., Eason, I. R., Breukink, E., Weingarth, M., & Wylie, B. J. (2024). Cooperative Gating of a K^+ Channel by Unmodified Biological Anionic Lipids Viewed by Solid-State NMR Spectroscopy. *Journal of the American Chemical Society*, *146*(7), 4421–4432. https://doi.org/10.1021/jacs.3c09266